Defining Asthma Phenotypes Using Hyperpolarized Gas MRI and CT

By

David G. Mummy

A dissertation submitted in partial fulfillment of

the requirements for the degree of

Doctor of Philosophy

(Biomedical Engineering)

at the

UNIVERSITY OF WISCONSIN-MADISON

2019

Date of final oral examination: 12/3/2018

The dissertation is approved by the following members of the Final Oral Committee:

Sean B. Fain, Professor, Biomedical Engineering, Medical Physics, and Radiology
Walter F. Block, Professor, Biomedical Engineering, Medical Physics
Oliver E. Wieben, Associate Professor, Biomedical Engineering and Medical Physics
Loren C. Denlinger, Associate Professor, School of Medicine
Ronald L. Sorkness, Professor, School of Pharmacy, School of Medicine
Scott K. Nagle, Assistant Professor, Radiology

Table of Contents

Defining Asthma Phenotypes Using HP Gas MRI and CT

David G. Mummy

A dissertation submitted in partial fulfillment of the requirements for the degree of

Doctor of Philosophy

(Biomedical Engineering)

Performed under the supervision of:

Sean B. Fain, Ph.D., Professor, Departments of Medical Physics, Biomedical Engineering, and Radiology

ABSTRACT

Magnetic resonance imaging (MRI) is an attractive modality for assessing structure-function relationships at relatively high resolution. This technique is particularly well suited for use in longitudinal studies and in pediatric populations where computed tomography (CT) or nuclear medicine-based technique may be contraindicated due to concerns about ionizing radiation. Applications of conventional MRI to the lung, however, present some unique challenges, among them rapid signal decay due to the remarkably high amount of interface between tissue and air in the lung (resulting in “magnetic susceptibility” and its consequent rapid spatial variations in the applied magnetic field); relatively low amount of signal-generating protons per unit volume; and cardiac and respiratory motion. Hyperpolarized helium-3 MRI (HP ^{3}He MRI) increases thermal helium gas signal by a

factor of 10,000, enabling rapid, direct imaging of inspired gas during a single breath-hold. Further, visualization and quantification of the ventilation patterns of inspired gas enables direct assessment (rather than inference) of function. Functional metrics derived from ventilation patterns can be used in isolation as biomarkers of obstructive physiology, or in tandem with other modalities to develop regional measurements and assess relationships to structural and other measures of obstructive physiology. In this work, we apply HP ^{3}He MRI to the study of asthma, a widespread, chronic lung disease of immense variety and complexity that has thus far proven difficult to assess and treat, much less cure, in all but the mildest cases. We first establish associations between a whole-lung metric based solely on ventilation patterns on HP ^{3}He MRI, specifically the ventilation defect percent (VDP), and a history of severe asthma attacks ("exacerbations") leading to emergency room visits or hospitalizations. After establishing this foundational relationship, we turn our attention to a comprehensive, prospective analysis including not only less severe exacerbations (i.e. those not necessarily associated with emergency care), but also the number of such exacerbations in the 2-year period following imaging. By incorporating exacerbation history and VDP, we create a "decision tree" model capable, with a high degree of significance, of predicting propensity for frequent exacerbation. We then consider VDP on a regional level and establish an association between airway mucus plugs (a common feature in asthma) seen on CT with localized measures of ventilation defects, indicating a possible role for HP ^{3}He MRI to monitor treatment response in patients receiving expensive biologic drugs that target the pathway of mucus plug formation. Finally, we delve into the realm of invasive measurements, and use regional measurements on HP ^{3}He MRI to guide bronchoscopic sampling in regions of ventilation

defect and well-ventilated control sites, the results of which provide insights into cellular activity localized to regions of defect. Overall, this dissertation firmly establishes the relationship between VDP on HP ^{3}He MRI and asthma exacerbation, and provides a framework for using regional measures of VDP to assess concomitant, and possibly causal, cellular activity and mechanisms of airway obstruction. Using these results and techniques for the further development and validation of imaging-based asthma phenotypes has the potential to inform and advance the development and evaluation of targeted therapies, to assess and select patients particularly suited to those therapies, and for longitudinal monitoring of treatment response.

To my parents, Beverly Geary and Mark Mummy

ACKNOWLEDGEMENTS

This work was financially supported by the Wisconsin Alumni Research Foundation (WARF) Technology Transfer Research Assistantship, the NIH/NHLBI R01 grants HL0808412 and HL091762 and U10 HL109168, and CTSA UL/TR000427. The data, resources, and expertise of the Severe Asthma Research Program formed the cornerstone on which this thesis was constructed.

Also *sine qua non* to this effort was my advisor, Dr. Sean Fain, whose support and guidance made this dissertation possible. Any and all novelty evidenced in this work is due in no small part to his ability to instigate and encourage inroads into particularly fruitful avenues of inquiry, and to nudge my highly enthusiastic but invariably half-baked ideas back into the realm of reality. Whatever ability I have gained in scientific writing, understanding my work in the broader clinical context, and incisive appraisal of new approaches and results, is wholly attributable to his mentorship. I have also been afforded a more than deserved opportunity to attend conferences and present my work and benefited greatly from Dr. Fain's extensive network in the field and his constant willingness to let me blunder into various communications and collaborations with researchers outside the lab. I am grateful for these and myriad other unenumerated benefits of Dr. Fain's support, guidance, and faith in my abilities.

Thank you to all of my committee members, Drs. Ron Sorkness, Loren Denlinger, Scott Nagle, Walter Block, and Oliver Wieben, for their guidance and availability throughout my tenure at UW-Madison. I have been tremendously fortunate in having the opportunity to benefit from their expertise and support, and the ability to state that I have

had both numerous and (from my perspective, at least!) greatly beneficial and enjoyable interactions with each and every one of them is something I do not take for granted.

Also utterly indispensable to this work was Michael Evans, MS, whose expertise in statistics and related programming elevated the significance of this work to a level far above that which it would have otherwise been mired. I have not only benefited from his guidance, modeling skills, and consistent responsiveness in the creation of this work, but by observing and implementing the techniques he has suggested and defined, I have developed a toolkit I will rely and build on extensively in my career going forward.

At the risk of sounding repetitive, but not wishing to understate the level upon which this work was built upon the foundations laid by others, I would also like to single out Drs. Wei Zha and Fain Lab alumnus Stanley Kruger for specific thanks in developing the essential foundational tools used in this work for analysis of HP ^{3}He MRI images, and for their help in implementing and troubleshooting the software nuts and bolts that provided the data building blocks of these studies.

Any acknowledgement would be incomplete without mentioning the invaluable support of my colleagues in the Fain Lab, including Drs. Robert Cadman, Andrew Hahn, and Annelise Malkus, and my fellow students Jeff Kammerman, Katie Carey, and Luis Torres, and Dr. Ben Cox, but especially Drs. Kai Ludwig and Erin Macdonald, whose warm friendship, optimism, and kindness from our beginnings as naïve first-years to the present, and I am wholly confident, extending far into the future, has been a particular and meaningful highlight of my time at UW-Madison. In the medical physics sphere outside of the Fain Lab, I have also enjoyed too many friendships to mention here, including Jacob

Macdonald, Xiaoke Wang, Christie Lin, Ante Zhu, Carson Hoffman, and Drs. T.J. Colgan, Curtis Wiens, and Gesine Knobloch.

Finally, and most important of all, I am grateful for the love and unconditional support of my parents, Mark Mummy, and Beverly Geary, my sister Linda Mummy, and brother-in-law Virya Ratanasangpunth, and, although she may be somewhat unaware of it, my young niece Nora Mummy. I would be nothing without the examples of hard work, integrity, kindness, and importance of serving in some small way a greater good that they exhibit on a daily basis, and their encouragement of my untethered dreams, advice on bringing those dreams about, and tolerance of my many shortcomings. This dissertation is wholly a result of their example and I can only hope to reflect these values as I move forward with my career and find my place in the world.

LIST OF FIGURES

LIST OF TABLES

LIST OF ABBREVIATIONS

AHR – Airway Hyperresponsiveness
AUC – Area Under Curve
BAL – Bronchoalveolar Lavage
BD -- Bronchodilator
CI – Confidence Interval
COPD – Chronic Obstructive Pulmonary Disease
CT – Computed Tomography
DWI – Diffusion-weighted Imaging
ED – Emergency Department
FeNO – Fractional Exhaled Nitric Oxide
FEV1 – Forced Expiratory Volume in One Second
FRC – Functional Residual Capacity
FVC – Forced Vital Capacity
HC – Histochemical
H&E – Hematoxylin and Eosin
HIPAA – Health Insurance Portability and Accountability Act
HP – Hyperpolarized
HU – Hounsfield Units
IHC – Immunohistochemical
IRB – Institutional Review Board
MDCT – Multidetector CT
MRI – Magnetic Resonance Imaging

NMR – Nuclear Magnetic Resonance
OCS – Oral Corticosteroid
OE – Oxygen Enhanced
OR – Odds Ratio
PAS – Periodic Acid-Schiff
PET – Positron Emission Tomography
PP – Percent Predicted
ROC – Receiver Operating Characteristic
RA-856 – Relative Area Under 856
ROI – Region of Interest
RF – Radiofrequency
RV – Residual Volume
SARP – Severe Asthma Research Program
SEOP – Spin-exchange Optical Pumping
SNR – Signal-to-noise Ratio
SPECT – Single-photon Emission Computed Tomography
TLC – Total Lung Capacity
VDP – Ventilation Defect Percent

INTRODUCTION

1.1 MOTIVATION

Magnetic resonance imaging (MRI) is capable of safely assessing structure-function relationships at relatively high resolution. This technique is particularly well suited for use in longitudinal studies and in pediatric populations where computed tomography (CT) or nuclear medicine-based technique may be contraindicated due to concerns about ionizing radiation. Applications of conventional MRI to the lung, however, present some unique challenges, among them rapid signal decay due to the remarkably high amount of interface between tissue and air in the lung resulting in “magnetic susceptibility” and its consequent rapid spatial variations in the applied magnetic field; relatively low amount of signal-generating protons per unit volume; and cardiac and respiratory motion. Hyperpolarized helium-3 MRI (HP ^{3}He MRI) increases thermal helium gas signal by a factor of 10,000, enabling rapid, direct imaging of inspired gas during a single breath-hold. Further, visualization and quantification of the ventilation patterns of inspired gas enables direct assessment, rather than inference, of function.

Asthma is a chronic, complex, and widespread disease with a growing array of treatment options, including promising, but very costly, monoclonal antibodies collectively known as “biologics”. An asthma attack (“exacerbation”) can result in a full range of outcomes, from a simple doctor’s visit to a trip to the emergency department, hospital admission, and in the worst cases may prove fatal. There is thus a significant need for techniques that can assess propensity for exacerbation and suitability for a particular

therapy, and monitor treatment response. Such techniques would prove similarly useful in the development and evaluation of targeted therapies. This dissertation lays the groundwork for lung ventilation imaging on HP ^{3}He MRI as a basis of such a technique or range of techniques.

1.2 OBJECTIVES

We seek to identify biomarkers on HP ^{3}He MRI associated with clinical outcomes and with localized measures of structure and function in asthma. We define three specific aims towards this end:

> **Aim 1.** Assess associations between ventilation defect extent and asthma exacerbation, both retrospectively and prospectively, developing and implementing software tools and workflows as required.
>
> **Aim 2.** Use regional measures of HP ^{3}He MRI to assess the functional significance of localized biomarkers of airway obstruction observed on other modalities. Apply this framework to regional measures of mucus plugging observed on CT.
>
> **Aim 3.** Develop and implement a methodology for assessing cellular activity in regions of ventilation defect vs. well-ventilated control sites by means of image-guided bronchoscopy.

Proposed future work will further develop biomarkers derived from HP ^{3}He MRI for use as measurements of exacerbation propensity and treatment response (e.g. a secondary endpoint in clinical trials), and as a tool for the development and evaluation of therapies targeting a specific mechanism of obstruction; and ultimately, constructing a phenotype

space in which these attributes can be assessed concurrently, providing a “holistic” picture of disease presentation and indicated interventions for each specific patient.

1.3 INNOVATION

The innovation of this work is three-fold. First, this is to our knowledge the first-time ventilation defect extent on HP gas imaging has been correlated with asthma exacerbation in a large-scale population of asthmatics, thereby establishing this association for future HP gas studies of asthma to rely on going forward. This effort involved both use of existing data (a retrospective analysis) and applying new tools developed in our lab to analyze image data in a prospective study, a challenge technologically, logistically, and statistically.

Second, we develop a technical pipeline for registering CT anatomical masks with HP ^{3}He MRI, thereby calculating ventilation defect extent by lung lobe and by the lung volumes that comprise the lobes, known as “segments.” Compared to whole-lung analysis or independent biomarkers, coupling localized biomarkers of airway structure and obstruction (including, but not limited to, biomarkers derived from CT itself), with ventilation defects allows for a more refined assessment of the functional significance of these biomarkers. Considerable time and effort were put into the workflow to make it reliable, robust, and suitable for replication at other lung imaging research sites.

Third, we develop a pipeline from “Gas Images to Cell Counts” for using regional ventilation patterns on HP ^{3}He MRI to guide bronchoscopy, and then evaluate the resulting samples for biomarkers of airway injury, inflammatory response, and cellular proliferation. This significant effort involved gaining an understanding of the tasks that

needed to be accomplished, marshaling the necessary expertise and equipment, developing an image analysis workflow, logistical management of physical and digitized samples, and a great deal of troubleshooting. However, our lab is now preparing to publish this pipeline and implement the methodology on a larger population of asthmatic subjects.

1.4 SUMMARY OF CHAPTERS

We begin with a brief introduction of the clinical presentation and treatment of asthma and an overview of functional lung imaging with a focus on hyperpolarized gas techniques; proceed to an overview of the two study populations underpinning this work; and finally, lay out the results of four studies addressing the above aims.

Chapter 2. An introduction to asthma and specific mechanisms of airway obstruction. Functional lung imaging, including CT, nuclear medicine, and MRI. Hyperpolarized gas imaging in MRI.

Chapter 3. Descriptions of datasets from two separate populations used in this study, “Retrospective” and “Longitudinal.” Basic population characteristics, and methods common to all studies.

Chapter 4. Ventilation defects on HP ^{3}He MRI are associated with a history of severe exacerbation (Retrospective population).

Chapter 5. Ventilation defects on HP ^{3}He MRI are predictive of exacerbation frequency in the two years following imaging (Longitudinal population).

2 BACKGROUND

2.1 INTRODUCTION

Asthma is a major cause of morbidity and health care utilization, and it has been estimated that over 600 million people worldwide are affected by some form of the disease. Disease prevalence is increasing, and over 7 million children have asthma in the United States alone [2].

Medication burden, asthma symptoms, and exacerbation history are typically used in tandem with spirometry to make a clinical assessment of asthma disease severity [3]. The primary clinical means of quantitatively characterizing asthma is spirometry, specifically measurements of forced expiratory volume in one second (FEV_1) and the ratio of FEV_1 to forced vital capacity (FVC) [3]. Asthma severity on spirometry is typically determined by the amount of decrease relative to predicted values of FEV_1, which reflects both airflow limitation and air trapping, and FEV_1/FVC, which reflects airflow limitation normalized to the amount of trapping [4]. Plethysmography is also employed clinically, although less frequently than spirometry, and can be used to determine absolute lung volumes, including residual volume (RV) , functional residual capacity (FRC), and total lung capacity (TLC) [5].

Despite the prevalence of asthma and the breadth of modalities available for the assessment of lung function, the complexity and heterogeneity of the disease have made it resistant to efforts to move treatment approaches beyond a broadly applied, one-dimensional scale of progressively escalating treatment. The development of clinically

meaningful disease phenotypes could enable improved methods of prognosis and guide the use of specific, targeted therapies. Recent developments of targeted biologic therapies [6] have precipitated the need to discriminate asthma subtypes in a clinical setting based on specific mechanisms underlying airway obstruction and thus reduced lung function. However, while multiple mechanistic phenotypes have been proposed and are currently undergoing investigating and refinement [7, 8], no standardized diagnostic framework has yet emerged.

Hyperpolarized gas MRI can be used to directly visualize the distribution of gas in the lungs using either HP ^{3}He [9] or ^{129}Xe [10]. The observed patterns of gas distribution ("ventilation heterogeneity") afford opportunities for assessing disease extent and progression, response to inhaled bronchodilator, and functional consequences of regional biomarkers of airway obstruction measured using other modalities. This methodology enables a more refined characterization of obstructive biomarkers than what is possible using the whole-lung tests that are the current clinical standard, and lay the groundwork for potentially clinically useful imaging-based phenotypes and the development and evaluation of targeted therapies.

2.2 Mechanisms of Airway Obstruction in Asthma

Asthma is a chronic condition characterized by predominately reversible airway obstruction. Symptoms of asthma are highly variable but may include coughing, wheezing, and chest tightness, or simply a feeling of breathlessness [3]. Acute episodes of airway obstruction may be triggered by stimuli such as respiratory viral infections, exposure to allergens, or exercise, which are superimposed on an underlying chronic inflammatory

process that renders the airways hyperresponsive to perturbations that in normal airways would evoke a negligible response. Treatments to ease obstruction primarily include bronchodilators to relax airway smooth muscle, and anti-inflammatory drugs such as corticosteroids; the latter are known to have long-term side effects [3].

The generally reversible airway obstruction that is the defining characteristic of asthma is the result of a range of complex, interrelated stimuli and pathologies. Thus, there is no single causal pathway leading to airflow obstruction, but rather a combination of phenomena that combine in various ways to impede airflow (Figure 1.1).

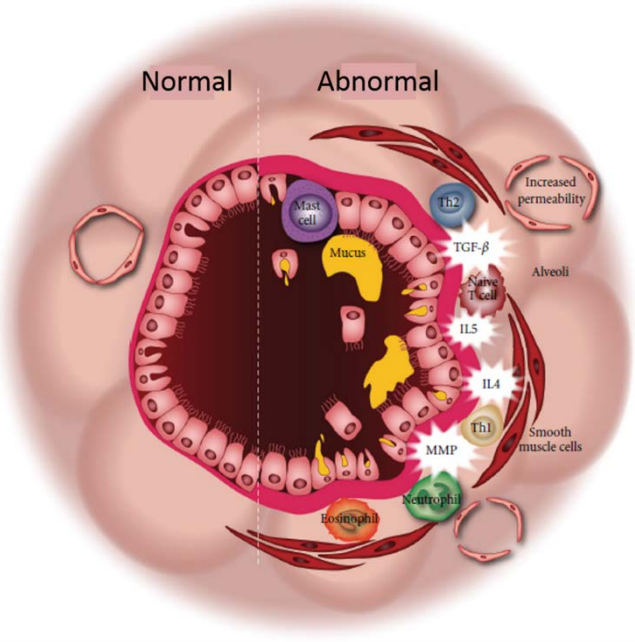

Figure 1.1. *Pathophysiological processes governing airway injury and remodeling in asthma. Basal membrane thickening and smooth-muscle hypertrophy and hyperreactivity are believed to occur due to chronic injury and airway remodeling. Adapted from A. Shifren, et al. J Allergy (Cairo). 2012;2012:316049.*

These obstructive mechanisms occur heterogeneously across asthmatics and within the lungs of an individual asthmatic, but one common feature across asthmatic patients is *airway hyperresponsiveness* (AHR), an overreaction of airway smooth muscle to environmental exposures, which causes bronchoconstriction and thus airflow limitation [3, 11].

To gain a better understanding of the relative roles played by obstructive pathologies in disease severity, progression, and response to therapy, it is desirable to study them not only in isolation but also in the context of the overall makeup of the disease pattern presenting in an individual subject, and to assess functional consequences of airway obstruction using spatially overlapping measures of ventilation. The use of imaging, particularly CT in conjunction with HP ^{3}He MRI, provides a means of linking localized obstructive mechanisms with the impeded airflow and reduced lung function that is their gestalt.

2.3 Functional Imaging of The Asthmatic Lung: An Overview

2.3.1 CT

The standard clinical imaging modality for the assessment of lung disease is multidetector CT (MDCT), which, though providing high contrast and resolution in the airways and parenchyma, is not readily amenable to direct measurements of function. Ionizing radiation further complicates the use of CT, often limiting or precluding its use in pediatric populations and longitudinal studies [12, 13], both of which are common in asthma research.

High resolution lung images on CT nonetheless play a valuable role in asthma research. The high level of detail allows for automated detection of lung fissures and segmentation of the airway tree to multiple branches. Commercial software such as VIDA (VIDA Diagnostics, Coralville IA) performs these tasks and produces anatomic masks identifying lung lobes and sublobar bronchopulmonary segments. Airway obstruction due to mucus hypersecretion ("mucus plugging") can also be visualized on CT in the central airways [14]. Interfaces between these techniques and the use of HP gas MRI in asthma will be described in detail in the chapters ahead.

2.3.2 Nuclear Medicine

Techniques based on nuclear medicine are used clinically to directly measure ventilation patterns, including single-photon emitted tomography (SPECT), nuclear scintigraphy with an inhaled technegas (i.e. technetium(Tc)-99m labeled aerosol) or ^{133}Xe, and $^{13}N_2$ gas positron emission tomography (PET) [15-17]. However, limitations in resolution, coverage, and signal-to-noise ratio (SNR), and once again, concerns about ionizing radiation, have kept these techniques out of mainstream research use in asthma.

2.3.3 MRI

Various gas contrast agents have been used to enable functional imaging of the lung using MRI. Oxygen-enhanced (OE) T1 mapping techniques can enable assessment of ventilation patterns by taking advantage of the paramagnetic effects of oxygen gas dissolved in the blood [18, 19]. These techniques use images acquired under alternating hyperoxic and normoxic conditions to highlight signal enhancement from the hyperoxic gas dissolved in vasculature that interfaces with well-ventilated regions of the lung. Though OE imaging has undergone significant use in research studies of obstructive lung

disease, and the ready availability of oxygen gas makes it highly amendable to clinical translation, it has not yet been widely applied to asthma even in the research setting.

Fluorinated gas MRI has been used to measure ventilation as far back as 1984 [20], though the technique did not become widespread in the research setting until the late 1990's. The ^{19}F isotope of fluorine is 100% naturally abundant and is visible on MRI at frequencies near that of standard (proton) MRI due to the similar gyromagnetic ratios between the ^{19}F and ^{1}H nuclei, both of which make it an attractive option for ventilation imaging [21]. Fluorinated gas MRI has recently been shown to be a feasible option for imaging asthma [22], and holds promise for significant applications in this area in the future.

The most widely used MRI contrast agent in the imaging of asthma, however, and the foundational technique in this dissertation, has been hyperpolarized gas. This technique and its applications are laid out in detail in the section that follows.

2.4 Hyperpolarized Gas Imaging In Asthma

Hyperpolarized gas MRI provides a means of directly visualizing gas distribution in the lung [23, 24] without the use of ionizing radiation present in CT, PET, and SPECT functional lung imaging. The resulting images are particularly useful in assessing ventilation heterogeneity in obstructive lung diseases such as asthma and chronic obstructive pulmonary disease (COPD), as these images highlight regions of low signal ("ventilation defects") distal to airway obstruction [25].

HP ^{3}He MRI of the lungs has been shown to be a robust and reproducible means of assessing ventilation defects in asthma, which in turn have been associated with areas of airway obstruction and air trapping [26, 27]. The most common metric for measuring

defect extent is the ventilation defect percent (VDP), which is calculated on HP ^{3}He MRI by segmenting regions of ventilation defect and lung boundaries and then dividing defect volume by segmental, lobar, or total lung volume [26, 28-30].

The versatility of HP gas MRI is further demonstrated by several additional unique applications: the use of diffusion-weighted imaging (DWI) to probe lung microstructure [31-33], and the ability to discriminate additional ^{129}Xe gas phases including absorption into the gas barrier and subsequent dissolution into the bloodstream [34-36].

2.4.1 Technical Methods

While ^{3}He and ^{129}Xe nuclei are both nuclear magnetic resonance (NMR) active and thus can be visualized using broadband MRI, the net magnetic moment of both gases as determined by the Boltzmann distribution at thermal equilibrium is too low to allow for imaging at the timescales required for lung applications. However, by using special equipment to excite the gas into a hyperpolarized state via the method of metastability [37] or the spin-exchange optical pumping (SEOP) technique developed by Walker and Happer [38], the net magnetic moment of the gas can be temporarily increased by multiple orders of magnitude, enabling imaging of ventilation over as short a period as a single 12-20 second breathhold.

The hyperpolarization technique demands significant investment in equipment, personnel training, maintainence, and time, all of which have combined to limit proposals for putative clinical applications.

3 STUDY POPULATIONS AND IMAGING METHODS

This work is drawn from two asthma study populations, the first oriented primarily around one visit with a significant retrospective component (the “Retrospective” population) and the second with a multiple-visit, prospective study design (“Longitudinal”). This section will broadly describe both populations and corresponding imaging methods so that they may be referred to succinctly in the course of describing the analyses and results that make up this dissertation.

3.1 “RETROSPECTIVE” STUDY

3.1.1 Population

This study population (N = 102, 64 female, mean age 29.2 ± 11.9 yrs), hereafter referred to as the “Retrospective” population, was drawn from the Viral Induced Asthma Exacerbation (VIAX) [39] and Severe Asthma Research Program (SARP) I-II [40] populations All studies were compliant with the Health Insurance Portability and Accountability Act (HIPAA) and approved by the relevant Institutional Review Board (IRB) (H-2002-296, H-2005-0070, H-2006-0338). Written informed consent was obtained from all research subjects. Subjects were approached consecutively, and MRI imaging was performed if consent was obtained.

The study population included healthy normal volunteers (N=11, 10.8%) and subjects with mild/moderate (N=75, 74.5%) or severe (N=16, 15.7%) asthma as defined by the SARP criteria [7]. These criteria use the American Thoracic Society workshop definition of severe asthma [41], which requires clinically observed signs of ongoing poor

asthma control despite treatment with high-dose corticosteroids; definitions of non-severe (i.e. mild and moderate) asthma are based primarily on measures of lung function and use of inhaled corticosteroids, a scheme previously used in national and international guidelines [7]. Subjects were excluded if an asthma exacerbation or respiratory complications had occurred within six weeks prior to imaging, or if airway obstruction was so severe that the subject was ineligible for MRI due to an IRB-imposed safety threshold (specifically, FEV_1 percent predicted [PP] < 60%).

HP ^{3}He MRI, proton (standard) MRI, and spirometry were obtained in all subjects. A subset of 88 (86.3%) of subjects underwent plethysmography to measure TLC and RV. Plethysmography was performed within 1-2 weeks of MRI.

3.1.2 MRI Imaging and Hardware

MRI studies were performed using a 1.5T Signa HDx GE scanner (GE Healthcare, Waukesha, WI) with a flexible wrap single-channel volume receiver coil (IGC Medical Advances, Milwaukee, WI) or a rigid-body single-channel volume receiver coil (Rapid Biomedical, Columbus, Ohio) depending on patient size. Both coils were tuned to operate at the resonant frequency of ^{3}He and decoupled from the body radiofrequency (RF) coil so that HP ^{3}He MRI and proton MRI could be acquired without moving the subject. The ^{3}He studies in this work were conducted using Polarean IGI.9600 polarizer (Polarean Imaging plc, Durham, NC) pictured in Figure 3.1 using the SEOP method described previously.

Figure 3.1. *The primary helium hyperpolarizer used in the studies in this work (Polarean model IGI.9600).*

A 4.5-mM dose of HP ^{3}He mixed with N_2 to 15% of the subject's TLC was prepared in a Tedlar™ bag purged of oxygen to slow T1 relaxation. The bag was delivered directly to the subject positioned supine in the scanner and the gas was inhaled from FRC through a small plastic tube attached to the bag, as illustrated in Figure 3.2.

Figure 3.2. *Example of home-made gas delivery apparatus (left) in use with the author pictured in MRI bore (right). Photo credit: Jeffrey Kammerman.*

Subjects were then instructed to hold their breath through a 16-20 second acquisition. Subjects were monitored continuously for blood oxygen saturation using a pulse oximeter to assess safety during the anoxic breath-hold and to ensure adequate recovery. Specific MRI acquisition parameters are summarized in Table B.

TABLE 3.1. HP ^{3}He MRI ACQUISITION PARAMETERS

MRI Parameter	Value
Pulse sequence	Fast 2D gradient-recalled echo (GRE)
TR/TE	7.7/4 ms
Flip angle	7°
Matrix	128 x 128 in-plane
FOV	40 cm
Reconstructed voxel dimension	1.56 x 1.56 x 15 mm
Slices	Sufficient to cover lung volume (12-18 slices)

Definition of abbreviations: TR – repetition time, TE – echo time, FOV – field of view.

3.1.3 Pulmonary Function Tests

Spirometry and plethysmography were performed according to American Thoracic Society/European Respiratory Society guidelines [42, 43] using a Jaeger MasterScreen plethysmograph and spirometry system (Care Fusion Respiratory, Yorba Linda, CA).

Percent predicted values for FEV_1, FVC, and FEV_1/FVC were generated by normalizing raw values for gender, race, age, and height to their predicted values using Hankinson standard equations [44]. Subjects withheld short-acting beta agonist treatments for 4 hours, long-acting beta agonist treatments for 12 hours, and other bronchodilator medications for an appropriate length of time prior to this exam to avoid pharmacologic interference with the measurements. For analysis purposes, the FEV_1 measurement acquired immediately before MRI was used as the subject's baseline FEV_1. The ratio of RV to TLC was normalized to obtain RV/TLC PP using the equations of Stocks and Quanjer [45].

3.1.4 History of Severe Clinical Outcomes

Severe outcomes were determined from records of emergency department (ED) visits and hospitalizations due to trouble breathing as gathered from written questionnaires completed by each subject at enrollment. These binary outcomes were defined by the presence of one or more incidents of the corresponding visit type, as recalled by the subject, at any time prior to study enrollment. These records were present for 94 (92.2%) of subjects.

3.1.5 Markers of Inflammatory Response

Samples of both sputum and peripheral blood were assessed to determine levels of eosinophils, neutrophils, and macrophages/monocytes. Cell differential was performed for sputum samples and counts for blood samples. "Total granulocytes" was defined as the sum of the values for eosinophils and neutrophils. Sputum samples were available for 93 (91.1%) of subjects and blood samples for 97 (95.1%) of subjects.

3.2 "LONGITUDINAL" POPULATION

3.2.1 Study Population

This study population was drawn from the UW-Madison and Washington University in St. Louis sites of the SARP III study [40]. The study was HIPAA-compliant and approved by the IRB (2012-0571), and written consent was obtained for all volunteers This study included either two or three imaging visits for each subject, as illustrated in Figure 3.3.

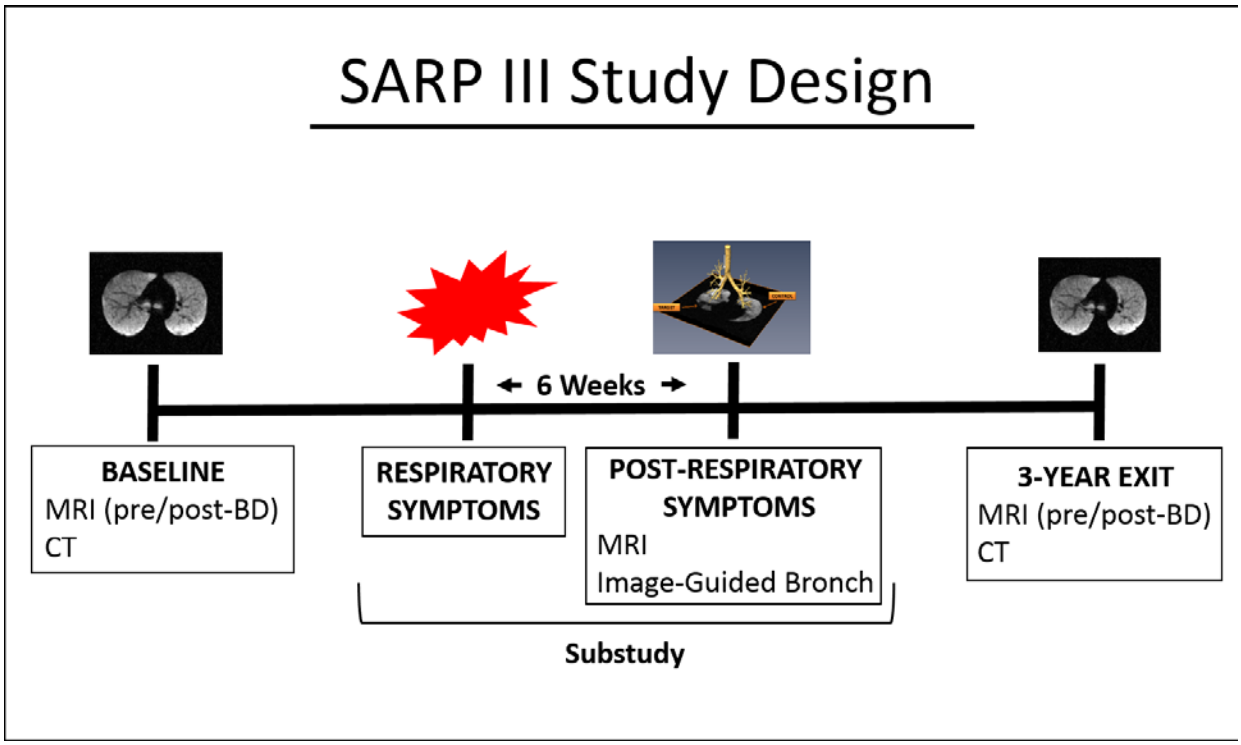

Figure 3.3. *SARPIII study design. Subjects underwent MRI (standard and HP gas) at baseline, along with CT when possible. A subset of subjects returned six weeks after experiencing respiratory symptoms for MRI and image-guided bronchoscopy. Subjects repeated the baseline imaging protocol at a three-year exit visit.*

Basic study population demographics and conventional clinical tests of lung function are summarized in Table 3.2.

	Mild/Moderate	Severe	All
N	31 (39.2%)	48 (60.8%)	79 (100.0%)
Sex	16 M (51.6%)	19 M (39.6%)	35 M (44.3%)
Age (yrs)	30.9 ± 17.1	41.1 ± 20.2	37.1 ± 19.6
BMI	25.1 ± 4.8	29.1 ± 6.2	27.5 ± 6.0
FEV1 PP pre-BD	91.6 [81.9 – 101.0]	77.0 [61.3 – 95.5]	83.2 [68.3 – 96.7]
FEV1 post-BD	97.0 [87.9 – 109.9]	83.4 [70.5 – 106.2]	92.6 [77.1 – 108.6]
FEV1/FVC pre-BD	90.4 [85.7 – 93.2]	86.5 [78.2 – 95.3]	88.8 [80.5 – 94.3]
FEV1/FVC post-BD	98.0 [92.4 – 100.7]	92.0 [83.2 – 99.4]	95.6 [87.8 – 100.1]
FVC pre-BD	100.6 [90.7 – 104.8]	85.3 [72.6 – 99.5]	94.8 [79.7 – 104.4]
FVC post-BD	103.8 [93.5 – 109.9]	89.7 [81.8 – 95.4]	97.2 [85.6 – 109.9]
FeNO	28.0 [16.0 – 42.0]	16.0 [11.0 – 26.0]	20.0 [12.0 – 33.5]
Blood eosinophils (counts/μL)	189.0 [107.0 – 278.0]	260.0 [167.0 – 502.0]	229.0 [141.8 – 424.0]
Sputum eosinophils (%)	0.8 [0.0 – 1.1]	0.5 [0.0 – 2.2]	0.55 [0.0 – 1.85]
Plasma IL5	15.7 [14.5 – 17.6]	19.3 [17.6 – 20.3]	17.8 [16.0 – 20.0]
Plasma IL6	0.8 [0.7 – 1.1]	1.6 [1.0 – 2.6]	1.1 [0.8 – 2.0]

Table 3.2. Summary of population characteristics. Results given as mean ± standard deviation or median [1st quartile – 3rd quartile]. Spirometry is shown both before and after bronchodilator (BD).

3.2.2 Pulmonary Function Tests

Spirometry was performed according to American Thoracic Society/European Respiratory Society guidelines [42, 43]. Percent predicted values for FEV_1, FVC, and FEV_1/FVC were generated using the Global Lung Function Initiative reference values [46].

3.2.3 Image Acquisition and MRI Hardware

Imaging was acquired in the same technical manner as in the “Retrospective” population, with the exception that inhaled gas volume was normalized to 14% of subject TLC rather than 15%. The protocol also differed from the Retrospective population in that HP gas imaging was performed both before and after administration of four puffs of albuterol, a β-agonist bronchodilator. CT was acquired post-bronchodilator only.

4 VENTILATION DEFECT PERCENT IN HELIUM-3 MRI IS ASSOCIATED WITH A HISTORY OF SEVERE OUTCOMES IN ASTHMA

4.1 ABSTRACT

4.1.1 Background

A small number of previous studies have looked at associations of imaging-based biomarkers with clinical outcomes in obstructive lung disease. However, the relationship between ventilation abnormalities on imaging and severe clinical outcomes in asthma remains poorly understood.

4.1.2 Objective

Hyperpolarized ^{3}He MRI provides regional measurements of airway obstruction, potentially enhancing sensitivity to clinical outcomes in asthma. We seek to assess possible associations between the VDP measured on HP ^{3}He MRI and severe clinical outcomes, and to compare these associations with those of conventional biomarkers of lung function and inflammation in asthma.

4.1.3 Methods

Study subjects were drawn from the “Retrospective” population described in Section 2. Study subjects (N = 102: 11 healthy volunteers, 75 mild/moderate asthmatics, and 16 severe asthmatics) underwent HP ^{3}He MRI, proton MRI, spirometry, and acquisition of blood and sputum inflammatory cells. A subset also underwent plethysmography.

Receiver operating characteristic (ROC) analysis and statistical associations were used to evaluate a suite of biomarkers as classifiers of a history of ED visits and hospitalizations due to trouble breathing. A machine learning algorithm was used to assess the relative contributions of factors in a multivariate model of severe outcomes.

4.1.4 Results

VDP was more strongly associated with ED visits (ROC area under curve [AUC] = 0.69, $p < 0.01$) and hospitalizations (AUC = 0.78, $p < 0.001$) than other biomarkers under consideration. In a multifactor gradient boosting machine model, VDP had over twice the relative influence in classifying history of severe outcomes than the next most influential factor.

4.1.5 Conclusion

VDP was more strongly associated with ED visits and hospitalizations from asthma exacerbation than were conventional biomarkers of lung function and inflammation.

4.2 INTRODUCTION

Asthma is characterized by variable airway obstruction associated with inflammation and remodeling. It is estimated to affect over 25 million people in the United States alone, and emergency department (ED) visits and hospitalizations due to severe exacerbation are a significant issue and driver of health care utilization [2]. The frequency and severity of exacerbations may also contribute to the rate of lung function decline. Understanding the factors leading to severe clinical outcomes is therefore important in advancing methods of disease prognosis and monitoring, and in the development and evaluation of targeted therapies.

Imaging-based biomarkers indicative of the extent and heterogeneity of airway obstruction have been associated with severe clinical outcomes in patients with obstructive lung disease [47-50]. Air trapping, using the relative area under -856 (RA-856) Hounsfield units (HU) [47] measure on CT at FRC, has been explored in a setting of severe asthma and found to be associated with a history of asthma-related hospitalizations, intensive care unit visits, and/or mechanical ventilation [48]. In addition, HP ^{3}He MRI measurements were recently compared to outcomes in COPD [49, 50], and were found to contribute significantly in models of the six-minute walk distance test, and to be predictive of severe pulmonary exacerbations.

The purpose of this work was to measure whole lung VDP on HP ^{3}He MRI in a cohort of asthma subjects with a spectrum of disease severity, and to evaluate associations of VDP with clinical outcomes indicative of exacerbation (“severe outcomes”). We also evaluated a suite of conventional biomarkers of lung function and obstruction and their respective associations with those same severe outcomes. We hypothesized that VDP-based measures of airway obstruction may be sensitive to asthma severity and instability, with the overall goal of developing VDP as a potential biomarker of severe exacerbation risk and as a means of decreasing the need for advanced health care utilization in asthma. HP gas imaging (whether ^{3}He or ^{129}Xe) may prove useful clinically in identifying patients susceptible to severe outcomes who require additional surveillance or intervention for improved asthma control [51], or for the evaluation of disease progression in targeted therapies.

4.3 METHODS

This study uses the “Retrospective” population described in Section 2.1.

4.3.1 Image Analysis

Total lung volume was determined from proton MRI using a semi-automated region growing algorithm. Ventilation defects on HP ^{3}He MRI were segmented manually using in-house software written in MATLAB (The MathWorks, Natick, MA) as previously described by Fain et al. [26]. This process resulted in lung volume and defect masks used to calculate the VDP.

4.3.2 Statistical Analysis

Differences in both FEV_1 PP and VDP across asthma severity groups were assessed pairwise using the Wilcoxon rank-sum test. Correlations between VDP and measures of lung function and inflammatory response (cell differential in sputum, cell counts in peripheral blood) were assessed using Spearman’s correlation. In asthmatic subjects (excluding healthy controls), associations between VDP and between VDP and hospitalizations were assessed using the Wilcoxon rank-sum test and ROC analysis, including measurements of ROC AUC. Analogous ROC analyses were performed using conventional measures of lung function (FEV_1 PP, FEV_1/FVC PP, RV/TLC PP) and biomarkers of inflammation in sputum and in peripheral blood. In the same asthmatic-only subpopulation, associations between VDP and three tiered “treatment levels” based on severe outcomes (“No treatment”, “ED visit without hospitalization”, “Hospitalization”) were assessed pairwise using the Wilcoxon rank-sum test. In order to estimate the relative contribution of each biomarker in classifying treatment level, a multivariate gradient boosting machine model [52] was fit using the gbm package [53]. This statistical

learning approach uses an ensemble of classification trees to predict treatment level, allowing for interactions among the biomarkers and providing a measure of the relative influence of each biomarker. All statistical analyses were performed in R version 3.2.3 (https://www.R-project.org/). The threshold for statistical significance was $p < 0.05$.

4.4 RESULTS

Pulmonary function test (PFT) and image-based measures of lung function for the study population are summarized in Table 4.1. Healthy subjects had significantly higher FEV_1/FVC PP compared with mild/moderate subjects ($p = 0.009$) and severe subjects ($p = 0.01$). Differences in FEV_1 PP and RV/TLC PP across groups were not significant.

TABLE 4.1. SUMMARY DEMOGRAPHICS AND LUNG FUNCTION STRATIFIED BY ASTHMA SEVERITY.

	Normals	Mild/Moderate	Severe	Significant Differences
N (row %)	11 (10.8%)	75 (73.5%)	16 (15.7%)	N/A
Sex (col %)	7 F (63.6%)	46 F (61.3%)	11 F (68.8%)	*(none)*
Age (yrs)	22.7 ± 3.6	28.8 ± 11.3	35.8 ± 15.3	Severe vs. normal (p=0.02)*
FEV_1 PP	99.0 [83.6 – 121.0]	92.0 [61.2 – 129.0]	88.1 [73.0 – 115.7]	*(none)*
FEV_1/FVC PP	101.0 [82.7 – 111.0]	92.5 [62.2 – 113.8]	89.6 [73.0 – 105.0]	M/M vs. normal (p=0.009) Severe vs. normal (p=0.01)
Whole Lung VDP (%)	0.2 [0.0 – 1.6]	0.9 [0 – 22.0]	2.8 [0 – 15.1]	M/M vs. normal (p=0.01)
RV/TLC PP	117.3 [92.9 – 132.1]	109.4 [67.9 – 184.0]	105.7 [81.3 – 162.1]	*(none)*
ED visit†	0 (0.0%)	32 (47.1%)	13 (86.7%)	Severe vs. M/M (p=0.006)*
Hospitalization†	0 (0.0%)	12 (16.0%)	7 (46.7%)	Severe vs. M/M (p=0.02)*

Definition of abbreviations: *FEV_1 – forced expiratory volume in one second, PP – percent predicted, FVC – forced vital capacity, VDP – ventilation defect percent, RV – residual volume, TLC – total lung capacity, ED – emergency department. Age is given as mean ± standard deviation, all other measurements as median [min – max]. †Percent of subjects with record of outcome. Significance tests are Wilcoxon rank-sum except *p-value of odds ratio. Significance tests for ED and hospitalization outcomes do not include normal subjects.*

Examples of typical MRI images used in this study are shown in Figure 4.1. Subjects with severe asthma and mild/moderate asthma had higher whole lung VDP than healthy normal subjects, as shown in Figure 4.2. Normal subjects were significantly different than mild/moderate asthmatics (p = 0.01) and severe asthmatics (p = 0.02), and VDP did not differ significantly between severe and mild/moderate asthma groups. Subjects with severe asthma reported a greater proportion of ED outcomes than subjects with mild/moderate asthma (odds ratio [OR] 7.3, 95% confidence interval [CI] 1.5-34.9, p = 0.006), and a greater proportion of hospitalizations (OR 4.1, 95% CI 1.2 – 13.4, p = 0.02).

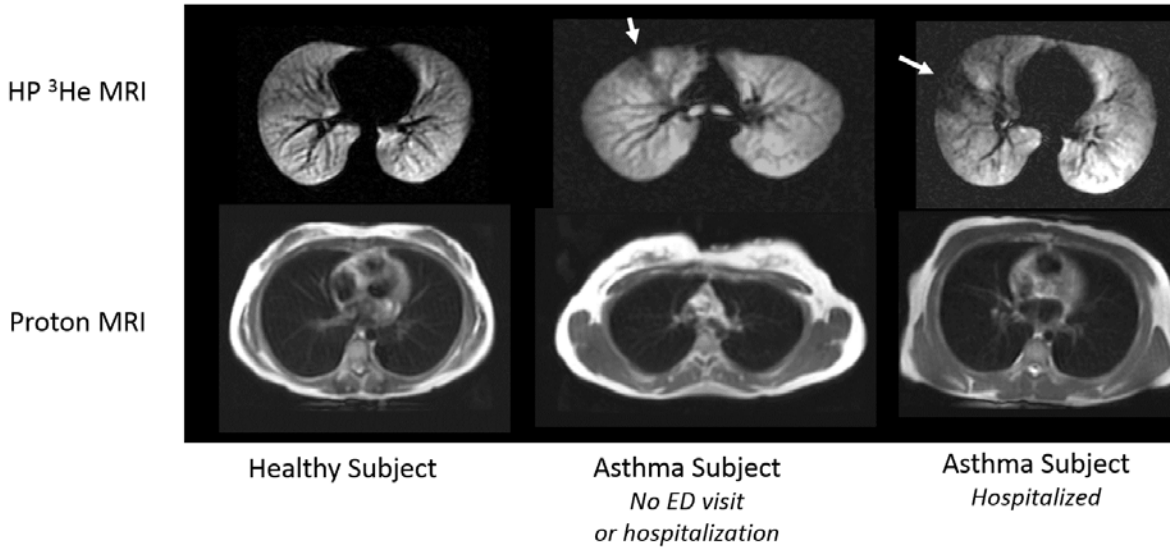

Figure 4.1. *Typical images of hyperpolarized ^{3}He MRI and corresponding proton MRI for a healthy control subject, an asthma subject with no record of severe exacerbation (emergency department [ED] visit or hospitalization), and an asthma subject who was hospitalized due to trouble breathing. Arrows indicate apparent ventilation defects. Ventilation defect percent (VDP): healthy, 0.88%; no exacerbation, 0.97%; hospitalized, 6.53%.*

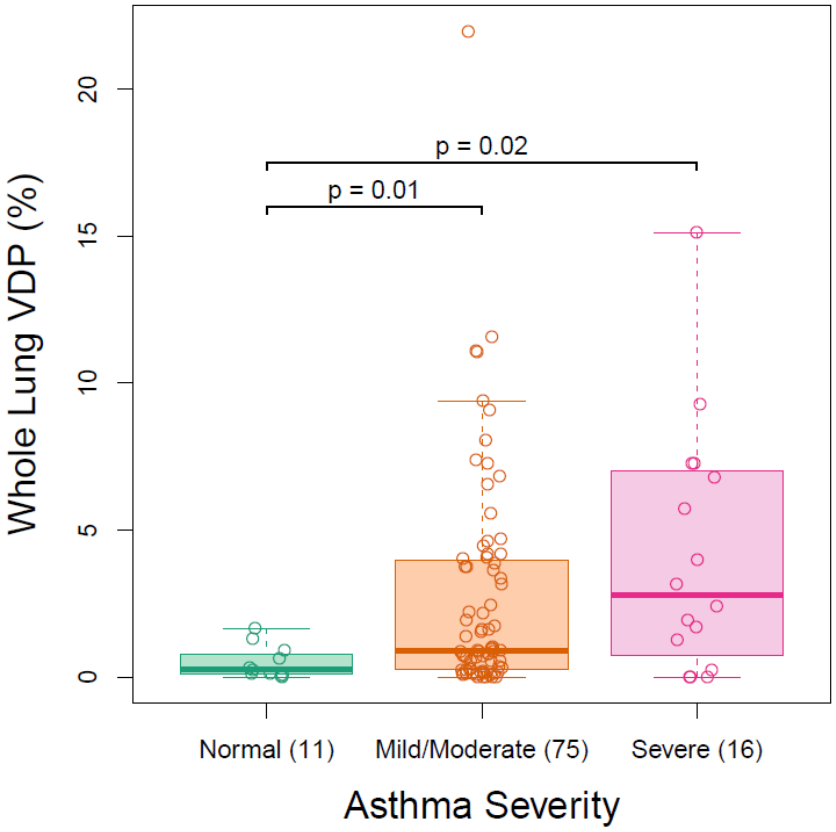

Figure 4.2. *Boxplot of median and interquartile range for whole lung ventilation defect percent (VDP) for normal and asthmatic subjects by clinically defined [1] asthma group. [Median, interquartile range] of whole lung VDP for normal, mild-moderate, and severe subjects was [0.24, 0.67], [0.90, 3.7], and [2.8, 5.9], respectively.*

4.4.1 Correlations between VDP and Other Biomarkers

Table 4.2 summarizes Spearman correlations between VDP and PFT's (FEV_1 PP, FEV_1/FVC PP, and RV/TLC PP), stratified by asthma severity. VDP was correlated with both FEV_1 PP and FEV_1/FVC PP in the full study population ($r = -0.32$, $p = 0.001$; $r = -0.54$, $p < 0.001$, respectively), as well as in the mild/moderate asthma subgroup ($r = -0.33$, $p < 0.004$; $r = -0.49$, $p < 0.001$). In the severe asthma group, VDP was correlated with FEV_1/FVC PP ($r = -0.52$, $p = 0.04$) only. In the normal subgroup, VDP was not correlated

with spirometry measurements. No statistically significant correlations were observed between VDP and RV/TLC PP.

TABLE 4.2 CORRELATION BETWEEN VENTILATION DEFECT PERCENT AND PULMONARY FUNCTION TESTS.

Asthma Severity	FEV_1 PP			FEV_1/FVC PP			RV/TLC PP		
	N	r	p	N	r	p	N	r	p
Normal	11	0.06	0.86	11	-0.45	0.17	8	-0.69	0.069
M/M	75	-0.33	0.004	70	-0.49	< 0.001	67	0.17	0.17
Severe	16	-0.22	0.42	16	-0.52	0.04	13	-0.06	0.84
Total	102	-0.32	0.001	97	-0.54	< 0.001	88	0.08	0.46

Definition of abbreviations: *FEV_1– forced expiratory volume in one second, PP – percent predicted, FVC – forced vital capacity, RV – residual volume, TLC – total lung capacity, M/M – mild to moderate, r - Spearman rank correlation coefficient, p – Spearman p-value.*

Table 4.3 summarizes Spearman correlations between VDP and a range of biomarkers of inflammatory response in both blood and sputum among the full study population. VDP was significantly correlated with peripheral blood eosinophil counts ($p < 0.001$) and sputum eosinophil differential ($p < 0.001$). No significant correlations were observed in monocytes/macrophages or neutrophils in either blood or sputum. Figure 4.3 shows scatterplots of the measures of lung function and inflammatory response that are listed in Table 4.3 as exhibiting significant correlations with VDP.

TABLE 4.3. CORRELATION BETWEEN VENTILATION DEFECT PERCENT AND BIOMARKERS OF INFLAMMATORY RESPONSE

Source	Biomarker	r	P
Peripheral Blood	Eosinophil count	0.39	< 0.001
	Monocyte count	0.06	0.53
	Neutrophil count	-0.02	0.85
Sputum	Eosinophil differential	0.36	< 0.001
	Macrophage differential	-0.03	0.79
	Neutrophil differential	-0.04	0.67

Definitions of abbreviations: *r – Spearman rank correlation coefficient; p – Spearman p-value.*

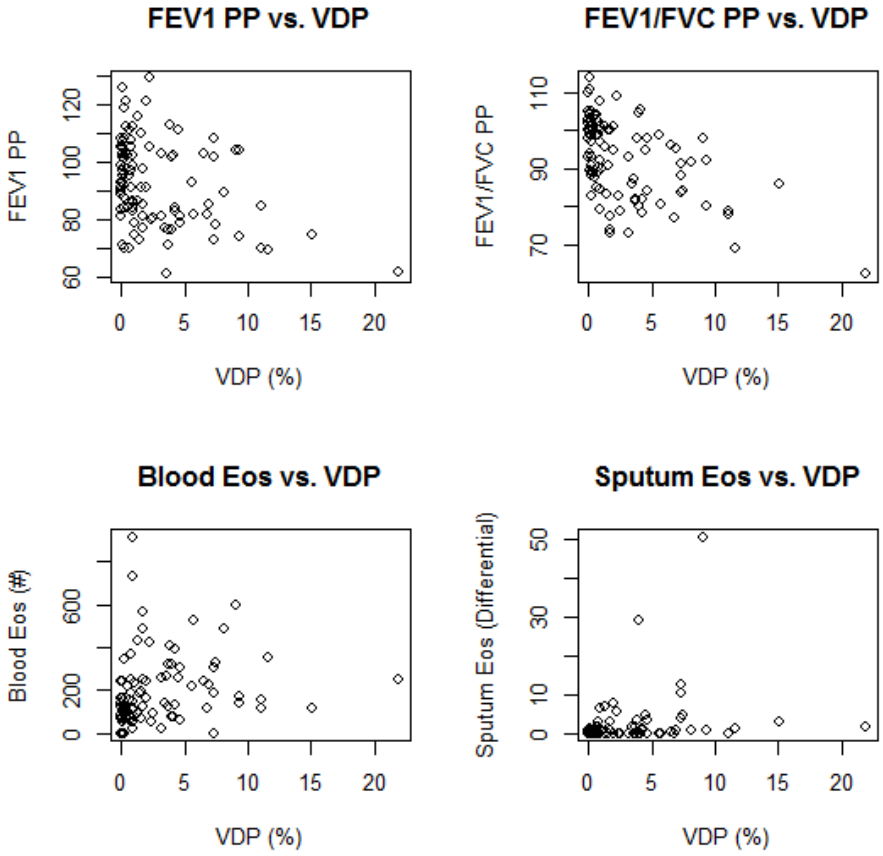

Figure 4.3. *Measures of lung function and biomarkers of inflammation exhibiting significant correlations with VDP.*

4.5 ASSOCIATIONS WITH SEVERE OUTCOMES

Table 4.4 shows ROC AUC values and Wilcoxon rank-sum test results assessing VDP and other biomarkers as indicators of severe outcomes among asthmatics. Corresponding ROC curves are shown in Figure 4.4. VDP was associated with ED visits (AUC = 0.69, $p < 0.01$) and hospitalizations (AUC = 0.78, $p < 0.001$). FEV_1/FVC PP was significantly associated with ED visits (ED = 0.64, $p = 0.04$), but not hospitalizations. None of the other conventional measures of lung function were significantly associated with either outcome.

TABLE 4.4 MEASURES OF INFLAMMATION AND LUNG FUNCTION AS INDICATORS OF SEVERE ASTHMA OUTCOMES.

		ED		Hospitalization	
Source	**Measurement**	**ROC AUC**	**p-value**	**ROC AUC**	**p-value**
Blood	Eosinophil count	0.62	0.07	0.66	0.04
	Neutrophil count	0.49	0.91	0.49	0.90
	Monocyte count	0.53	0.64	0.50	0.97
Sputum	Eosinophil differential	0.61	0.09	0.62	0.10
	Neutrophil differential	0.56	0.41	0.52	0.80
	Macrophage differential	0.53	0.70	0.55	0.50
Spirometry	FEV_1 PP	0.54	0.59	0.62	0.12
	FEV_1/FVC PP	0.64	0.039	0.61	0.16
Plethysmography	RV/TLC PP	0.56	0.39	0.49	0.99
MRI	VDP	0.69	0.004	0.78	< 0.001

Definitions of abbreviations: *ED – emergency department, ROC – receiver operating characteristic, AUC – area under curve, FEV_1 – forced expiratory volume in one second, PP – percent predicted, FVC – forced vital capacity, TLC – total lung capacity, VDP – ventilation defect percent, p – probability.*

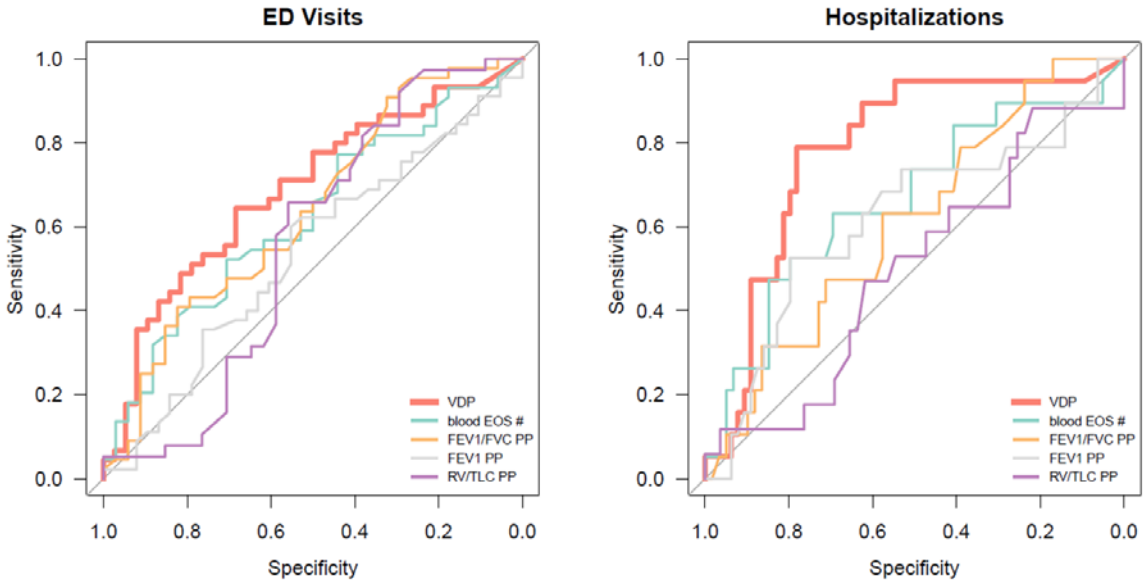

Figure 4.4. *Receiver operating characteristic (ROC) curves illustrating selected biomarkers of obstruction among asthmatic subjects as predictor of emergency department (ED) visits and hospitalizations. VDP – ventilation defect percent; EOS # – eosinophil count; FEV1 – forced expiratory volume in 1 second; FVC – forced vital capacity; PP – percent predicted; RV – residual volume; TLC – total lung capacity.*

Peripheral blood eosinophil counts were significantly associated with hospitalizations (AUC = 0.66, p = 0.035). Although not reaching significance, other measures of eosinophils in blood and sputum tended to be associated with hospitalizations ($p \leq 0.10$) with ROC AUC curve values greater than 0.6. None of the measures of neutrophils and macrophages/monocytes in blood or sputum were significantly associated with either clinical outcomes.

In a multivariate analysis incorporating all biomarkers under consideration, including VDP, measures of lung function, inflammatory response, age, and gender, the most informative indicator of severe outcomes was VDP, with over twice the relative influence compared to number of blood eosinophils, the next most informative biomarker (Figure 4.5).

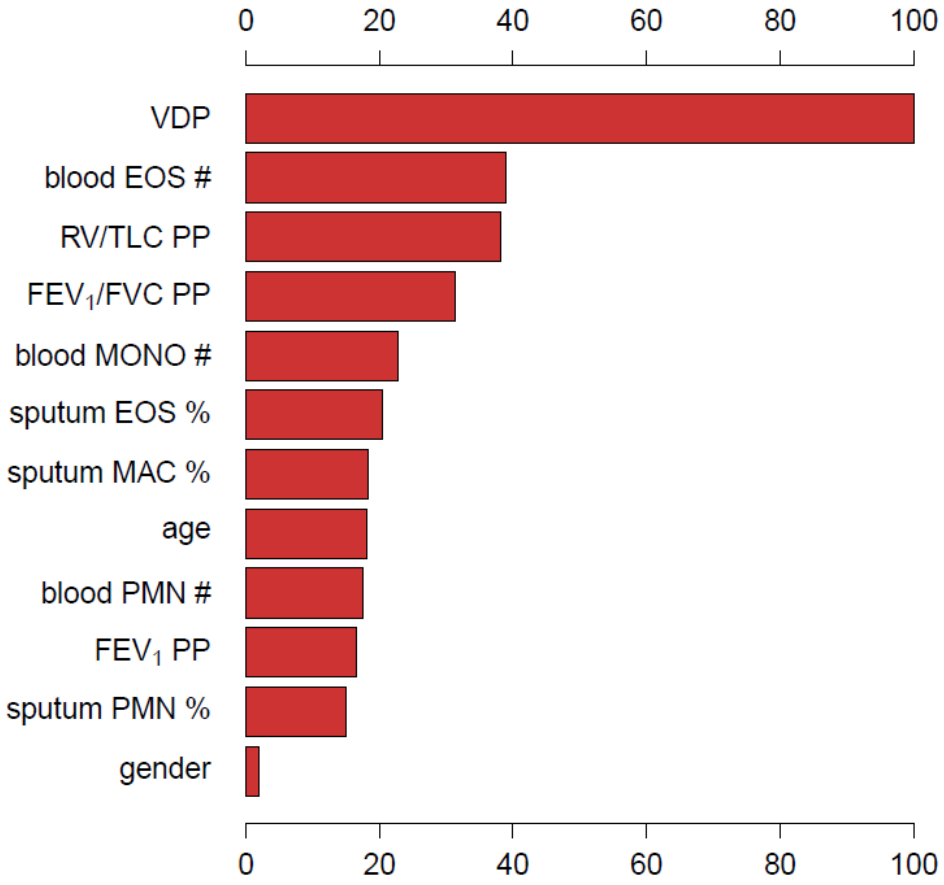

Figure 4.5. *Gradient boosting machine results showing ventilation defect percent (VDP) with highest relative influence over other factors in predicting severe outcomes. Horizontal axis indicates relative influence with VDP normalized to 100. EOS – eosinophil; RV – residual volume; TLC – total lung capacity; PP – percent predicted; FEV_1 – forced expiratory volume in one second; FVC – forced vital capacity; MAC – macrophage; PMN – neutrophil.*

The distribution of VDP values stratified by the three measures of outcome among asthmatics (none, N = 37; ED alone, N = 27; hospitalization, N = 19) together with example HP MRI images from each group are shown in Figure 4.6. Subjects who were hospitalized had higher median VDP (4.0%) than those who visited the ED alone (0.9%; hospitalized vs. ED-alone, $p < 0.005$) or did not require treatment (0.8%) (hospitalized vs.

no treatment, p < 0.001). VDP did not differ significantly between the ED-alone and no-treatment groups.

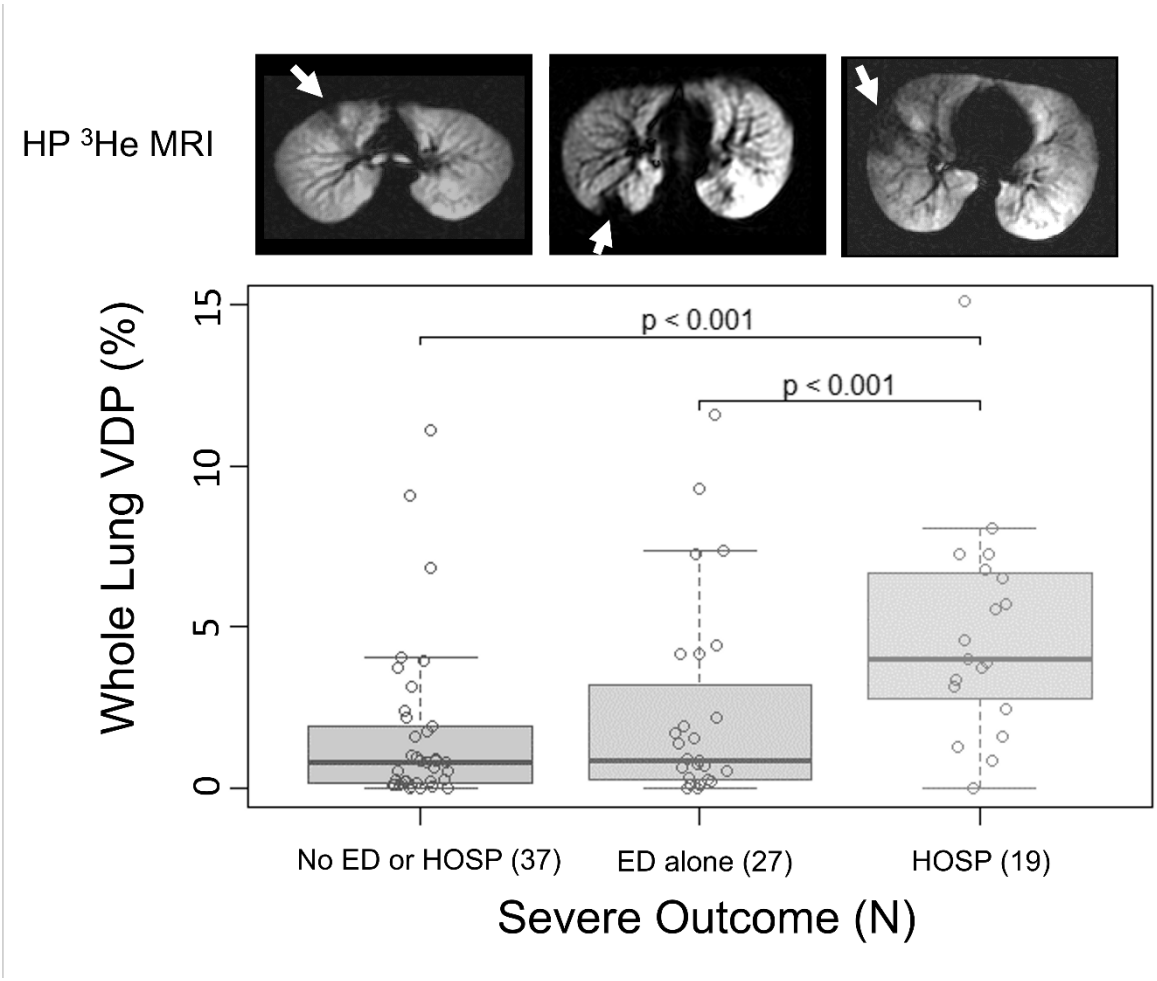

Figure 4.6 *Whole lung ventilation defect percent (VDP) vs. outcome group in asthmatic subjects. VDP [median, interquartile range]: No ED or hospitalization (HOSP), [0.78, 1.77]; ED alone, [0.85, 2.95]; HOSP, [4.0, 3.86]. Shown above are typical images of hyperpolarized ^{3}He MRI for subjects in corresponding outcome groups. Arrows indicate apparent ventilation defects. Ventilation defect percent (VDP): no ED or HOSP, 0.97%; ED alone, 1.93%; hospitalized, 6.53%.*

4.6 DISCUSSION

This study demonstrated that the ventilation defects observed on HP 3He MRI are associated with clinical outcomes indicative of severe asthma exacerbations. This result

is consistent with a related study that found VDP to be strongly associated with previous hospitalization in COPD [49]. The present work also confirms in a larger population of asthma subjects that VDP is increased with asthma severity relative to healthy normal subjects [26, 54]. Severe asthmatics in our study exhibited a substantially greater propensity for severe outcomes compared to mild/moderate asthmatics, indicating that the study population was a reasonable reflection of the severe asthma population observed clinically [40]. In combination, these results indicate that VDP warrants further study as an indicator of asthma instability and a possible imaging biomarker to help guide asthma management.

When modeling VDP as an indicator of both ED visits and hospitalizations using ROC analysis, AUC values for hospitalization were significantly higher than for ED visits (0.78 vs. 0.69 respectively). Figure 4.6 highlights the markedly higher VDP values among subjects who were admitted to the hospital and illustrates the comparative similarity in VDP distribution between the no-treatment and ED-alone subgroups. This is perhaps not surprising given that hospitalization is presumably indicative of a more acute exacerbation than an ED visit alone. Indeed, no significant association was found for VDP in subjects who visited the ED without a hospitalization (ED-alone), highlighting a possible role for VDP in identifying subjects prone to more severe exacerbations. Importantly, since VDP was associated with hospitalizations irrespective of clinical severity designation, and since hospitalizations were reported in 12/68 (17.6%) of subjects classified as mild/moderate under the SARP criteria, it is possible that improvements in prognostic techniques could indeed prove valuable in guiding disease surveillance and therapy in asthma.

VDP was also correlated with spirometric measures of airway obstruction, corroborating earlier findings by de Lange et al. [54] and Svenningsen et al. [25], and recent findings of Altes et a.l in childhood asthma [55]. As understood using the physiologic interpretation from Sorkness et al.[4], VDP exhibited a stronger correlation with airflow limitation (FEV_1/FVC PP) than with either air trapping (RV/TLC PP) or overall trapping and obstruction (FEV_1 PP). Lung volume on plethysmography was obtained up to two weeks after imaging, and thus day-to-day variation of air trapping may contribute to the lack of significant correlation between VDP and RV/TLC PP. However, since all measurements were obtained during a period of asthma stability, differences in timing should not affect the relationship between individual metrics and severe outcomes. The stronger correlation between VDP and FEV_1/FVC in our data is also in agreement with Kruger et al.[56], who found that FEV_1/FVC PP was also associated with disease severity as determined by the SARP criteria, whereas FEV_1 alone was not. These findings taken together suggest that central airway limitation may be the dominant obstructive mechanism associated with asthma-related ventilation defects identified via HP ^{3}He MRI. Moreover, this association of VDP with FEV_1/FVC PP showed a higher correlation coefficient in the severe asthma subgroup in our study.

Based on the ROC and multivariate analysis, VDP appears to be a superior indicator of severe outcomes than conventional PFT’s, suggesting that characterizing regional lung function via hyperpolarized gas imaging may be a useful tool for identifying subjects with unstable asthma. Importantly, measures of blood and sputum eosinophils were nearly as predictive of severe outcomes as VDP, and a combined approach may be more selective of patients with severe outcomes. If these findings are validated in an

independent cohort, the added refinement and specificity gained from using regional measures of lung function may provide an improved means of identifying asthma patients more refractory to therapy. Further, employing these measurements in a prospective study of asthma exacerbation could determine if VDP is a possible prospective predictor of severe outcomes in asthma. Phase III of the SARP study has recently concluded and will enable a more complete, prospective analysis (see Section 5). That study protocol includes HP ^{3}He MRI at both a baseline and 3-year exit visit; a subset of the population also underwent imaging following respiratory symptoms. Extensive longitudinal data on disease control, clinical assessment, and lung function were also obtained, making it possible to establish the association and persistence of VDP in the context of asthma stability and severity.

The use of VDP derived from HP gas MRI could complement conventional clinical designations of severity and biomarkers (e.g. serum and sputum inflammatory cells) associated with instability and severe exacerbation, enabling more accurate identification and surveillance of patients at high risk of severe exacerbation. Ultimately, this work is directed at refining the selection of patients for biologic drug therapies (e.g. mepolizumab, an IL-5 inhibitor) or bronchial thermoplasty.

It is noteworthy that the severe asthma population in our study excluded subjects with severely reduced lung function due to the IRB safety exclusion criteria present at the time of the study. As such, the lowest FEV_1 PP of any subject in the study was 61.2%. Therefore, the subgroup of severe asthma studied presented with an atypically mild airway obstruction relative to the general asthma population. This criterion led to similar distributions of lung function measures (i.e. plethysmography and spirometry) in severe

vs. mild/moderate asthmatics in this particular study population. Perhaps as a consequence, conventional PFT's (i.e. FEV_1/FVC) showed only a limited association with severe outcomes, with FEV_1 PP and RV/TLC showing no association at all. Despite this selection for less obstructive global physiology, VDP on MRI showed significant and substantive differences in the propensity for severe outcomes in these same subjects. Therefore, VDP appears to provide increased sensitivity and precision relative to other biomarkers in a study population consisting of more moderate disease, where it may aid in therapeutic decisions more typically encountered in the clinic.

4.7 LIMITATIONS

This study has several limitations. First, we have not accounted for the number or chronology of severe outcomes, only whether at least one instance of each outcome occurred at any time prior to study enrollment (additional outcomes data limited to the year prior to imaging were available, but the incidence rate of severe outcomes during this time period was too low to allow for meaningful analysis). Outcomes data were based on written questionnaires and depend on the ability of the subject to recall treatment history; incorporating medical records and including the frequency and timing of exacerbation events relative to imaging would likely allow us to make a more accurate description of clinical severity. Using the number of visits over a specific observation period would also strengthen the results, though this approach would require a sufficiently large subject population. In addition, future studies with access to post-imaging clinical outcomes would be able to assess VDP as a predictor of severe exacerbations, rather than being restricted to retrospective associations.

Second, the population predominantly consisted of mild/moderate asthmatics. A population with a greater number and proportion of severe asthmatics and healthy subjects as controls would allow for more statistical power and improve discernment of possible severity-related heterogeneity. Since the severe asthma study population was also significantly older than control subjects and limited to subjects with at least 60% FEV_1 PP, these findings are not generalizable to the full spectrum of asthma severity and may be biased by age-dependent factors. However, the VDP and inflammatory associations in this work are probably most relevant to this particular subgroup of asthmatics for whom disease is currently limited but may be progressing, and who may thus be best served clinically by a tool to assess their likelihood for severe exacerbation and disease progression. To further address concerns about age bias, we used a gradient boosting machine model that allows for a comparison of the relative influence of VDP in the model, and was also ranked below other factors, including spirometry, plethysmography, and biomarkers of inflammation.

4.8 CONCLUSION

This work demonstrates that VDP is more strongly associated with clinical outcomes of asthma exacerbation than are conventional pulmonary function tests or markers of inflammatory response, and that VDP shows promise as a biomarker associated with those severe outcomes.

We also characterized the correlations of VDP with other biomarkers. VDP was most strongly correlated with measurements of eosinophils in blood and sputum, and was

also strongly correlated with airflow limitation (FEV_1/FVC PP), and to a less extent, global trapping and obstruction together (FEV_1 PP), corroborating previous work in this area.

Although an HP MRI exam is currently more expensive than PFT's, a CT, or a blood/sputum test, the cost may be justified for clinical use if the results could aid in the prediction or prevention of a severe exacerbation leading to a hospital stay. Given these results, further study of VDP measured on HP gas MRI as a tool for identifying patients with unstable asthma and guiding targeted therapies is warranted and may prove to be a cost effective approach to improving patient outcomes.

5 VENTILATION DEFECT PERCENT IS PREDICTIVE OF ASTHMA EXACERBATION FREQUENCY

5.1 ABSTRACT

5.1.1 Rationale

Ventilation defects on hyperpolarized helium-3 magnetic resonance imaging (HP ^{3}He MRI) in asthma have been associated with severe exacerbation in both retrospective and prospective studies. However, these studies did not assess the utility of VDP as a predictor of asthma exacerbation frequency (i.e. cumulative exacerbations over a specified period of time). Incorporating history of recent exacerbation may also inform and improve models of VDP as a predictor of exacerbation frequency.

5.1.2 Methods

66 asthma subjects (27M 39F, 28 mild/moderate and 38 severe) drawn from the Severe Asthma Research Program (SARP) underwent HP ^{3}He MRI during a period of disease stability, and defect extent was measured using the ventilation defect percent (VDP). VDP was compared with spirometry and with blood and sputum eosinophils using Spearman's correlation. The number of asthma exacerbations was recorded prospectively over the two-year period following imaging. We used a Poisson regression tree model to assess associations between VDP and exacerbation frequency and estimate an optimal VDP threshold. We then expanded the model to include a binary indicator of a record of severe

(i.e. requiring systemic corticosteroid) exacerbation during the 12 months prior to imaging as an additional predictor of exacerbation frequency.

5.1.3 Results

Median [1Q – 3Q] VDP was 5.6% [2.6% - 13.6%] in severe subjects vs. 1.9% [0.55% - 3.0%] in mild/moderate subjects. VDP was negatively correlated with forced expiratory volume in 1 second (FEV1) percent predicted (PP), FEV1 divided by forced vital capacity (FVC) PP (FEV1/FVC PP), and FVC PP, and positively correlated with measurements of eosinophils in blood and sputum. A VDP threshold of 4.28% was selected based on maximum likelihood estimation of the regression tree model. Subjects with VDP exceeding the threshold (N = 30) had 1.5 [0.25 - 3.0] exacerbations vs. 0.0 [0.0 - 1.0] for subjects below the threshold (N = 36, Figure 1). The exacerbation frequency ratio for subjects above vs. below the VDP threshold was 2.8 (95% CI 1.6 - 5.2), p=0.001. By comparison, subjects classified as severe (N =38) had 1.0 [0.0 - 2.75] exacerbations vs. 0.0 [0.0 - 1.0] for mild/moderate subjects (N = 28), and the corresponding exacerbation frequency ratio was 2.4 (95% CI 1.3 - 4.9), p = 0.01. In the model incorporating both recent severe exacerbation and VDP as predictors of exacerbation frequency, we found that VDP above 4.28% (p=0.0006) and prior severe exacerbation (p=0.001) were each risk factors for increased exacerbation frequency. Importantly, among subjects without a recent severe exacerbation, those with VDP above the threshold (n=18) had more frequent exacerbations than those below (n=26) (exacerbation frequency ratio = 5.6, p<0.0001).

5.1.4 Discussion

We found that the ventilation defect percent (VDP) on hyperpolarized gas MRI is predictive of exacerbation frequency in the two years following imaging, corroborating previously published results [57] showing that VDP was associated with a history of severe exacerbation. We also found that severe exacerbation prior to imaging was an important mediator in models of VDP as a predictor of exacerbation frequency. These results suggest that measurements of VDP in the context of exacerbation history may enable a decision-tree based approach to monitoring treatment response both in individual subjects and in clinical trials, and for selecting patients in need of intensive therapy intervention.

5.1.5 Conclusion

VDP on HP ^{3}He MRI in asthma is predictive of exacerbation frequency over a two-year period following imaging, and these models are further improved by incorporating records of recent severe exacerbation. These results provide additional evidence for VDP as a possible clinical biomarker of propensity for severe outcomes in asthma.

5.2 INTRODUCTION

Image-based biomarkers on MRI and CT have been correlated with measures of lung function and outcomes in asthma and COPD, as presented in Section 3.1. In particular, ventilation defects in asthma are associated with a history of severe clinical outcomes [57] as presented in the previous section. Establishing VDP as a predictor of asthma exacerbation is useful in establishing VDP as a means of assessing disease severity, assessing suitability for targeted therapy, and evaluating efficacy in clinical trials. This

study extends the approach presented in the previous section to a prospective study of VDP as a predictor of asthma exacerbations and exacerbation frequency in a two-year period following baseline imaging, where an exacerbation is defined as three or more consecutive days of oral corticosteroid (OCS) use. Further, we incorporate history of recent severe exacerbation to inform and improve our model of VDP as a predictor of exacerbation frequency, where recent severe exacerbation was defined as systemic corticosteroid use in the year prior to imaging.

5.3 METHODS

Subjects in this study were drawn from the "Longitudinal" population as described in Section 3.2 and restricted to subjects with successful baseline HP ^{3}He MRI scans pre-bronchodilator and who remained enrolled for at least two years following baseline imaging. HP ^{3}He MRI was performed as described in Section 3.2.

5.3.1 Image Analysis

Proton MRI was registered to HP ^{3}He MRI using a 3D rigid registration algorithm implemented using the Advanced Normalization Tools packing (ANTs, http://stnava.github.io/ANTs/). The lung boundary on HP ^{3}He MRI was segmented with reference to the proton MRI and regions of ventilation defect were classified on HP ^{3}He MRI using the semi-automated algorithm developed by Zha et al. [58].

5.3.2 Statistical Methods

Correlations between VDP and clinical measures of lung function (spirometry and fractional inhaled nitric oxide [FeNO]) and plasma measurements of cytokines and of blood and sputum eosinophils were assessed using the Spearman correlation. We used

a Poisson regression tree model to assess associations between VDP and exacerbation frequency and estimate an optimal VDP threshold. We then expanded the model to include a binary indicator of a record of severe (i.e. requiring systemic corticosteroid) exacerbation during the 12 months prior to baseline imaging as an additional predictor of exacerbation frequency.

5.4 RESULTS

5.4.1 Study Population

A summary of population characteristics, including whole-lung VDP and 2-year exacerbations, is presented in Table 5.1.

	Mild/Moderate	Severe	All
N	28	38	66
Sex	14F (50.0%)	25 F (65.8%)	39 F (59.1%)
Age (yrs)	31.1 ± 17.4	42.8 ± 21.2	37.9 ± 20.4
BMI	24.5 [21.4 – 27.7]	28.5 [25.2 – 33.3]	27.3 [23.3 – 30.8]
FEV1 PP	89.6 [81.2 – 101.9]	75.6 [55.8 – 95.0]	82.7 [66.9 – 96.3]
FEV1/FVC PP	90.7 [85.9 – 94.0]	86.5 [78.6 – 93.7]	89.9 [81.5 – 93.7]
FVC PP	99.5 [88.6 – 104.8]	82.7 [71.0 – 97.8]	94.2 [78.8 – 103.5]
FeNO	26.5 [16.0 – 41.5]	14.0 [9.5 – 25.5]	20.0 [11.5 – 34.0]
Blood eosinophils (counts/μL)	198.5 [107.5 – 280.0]	309.5 [147.2 – 508.5]	229.5 [137.0 – 466.5]
Sputum eosinophils (%)	0.8 [0.0 – 1.1]	0.6 [0.1 – 3.2]	0.6 [0.0 – 2.0]
Plasma IL5	15.7 [14.5 – 17.6]	19.4 [17.6 – 20.3]	17.8 [16.0 – 20.1]
Plasma IL6	0.8 [0.7 – 1.1]	1.6 [1.0 – 2.6]	1.1 [0.8 – 1.7]
VDP (%)	2.0 [0.6 – 3.2]	5.9 [3.4 – 14.4]	3.64 [1.2 – 7.4]
Exacerbations	0.0 [0.0 – 1.0]	1.0 [0.0 – 2.8]	1.0 [0.0 – 2.0]

Table 5.1. Summary of population characteristics. Results given as mean ± standard deviation or median [1st quartile – 3rd quartile]. All measurements acquired prior to bronchodilator administration.

5.4.2 Correlations between VDP and Clinical Measures

Figure 5.1 illustrates VDP in severe vs. mild/moderate subjects. Median [1Q – 3Q] VDP is 5.6% [2.6% – 12.8%] in severe subjects vs. 1.5% [0.55% – 3.0%] in mild/moderate ($p < 0.0001$).

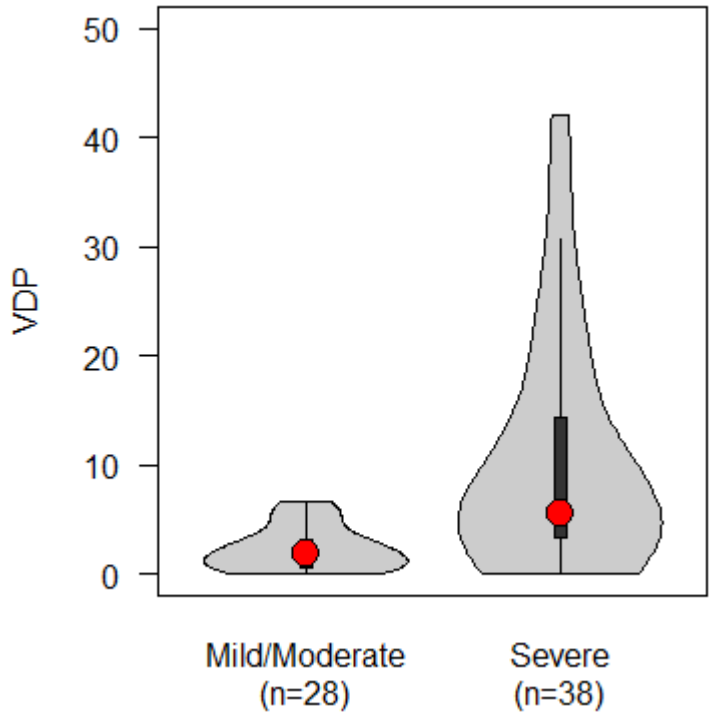

Figure 5.1. *VDP in mild/moderate vs. severe subjects. Median [1Q – 3Q] VDP is 5.6% [2.6% – 13.6%] in severe subjects vs. 1.9% [0.55% – 3.0%] in mild/moderate ($p < 0.0001$).*

Correlations between VDP and spirometry are summarized in Table L. VDP was not correlated with FeNO.

Clinical Measure	Correlation with VDP
FEV1 PP	r = -0.47, p < 0.0001
FEV1/FVC PP	r = -0.42, p < 0.001
FVC PP	r = -0.44, p < 0.0001
Sputum Eos	r = 0.31, p = 0.028
Blood Eos	r = 0.23, p = 0.047
Plasma IL-5	r = 0.51, p < 0.001
Plasma IL-6	r = 0.60, p < 0.0001

Table 5.2. Spearman's correlation between VDP and clinical measures of lung functions and inflammatory response.

5.4.3 VDP as a Predictor of Outcomes

5.4.3.1 ROC Analysis

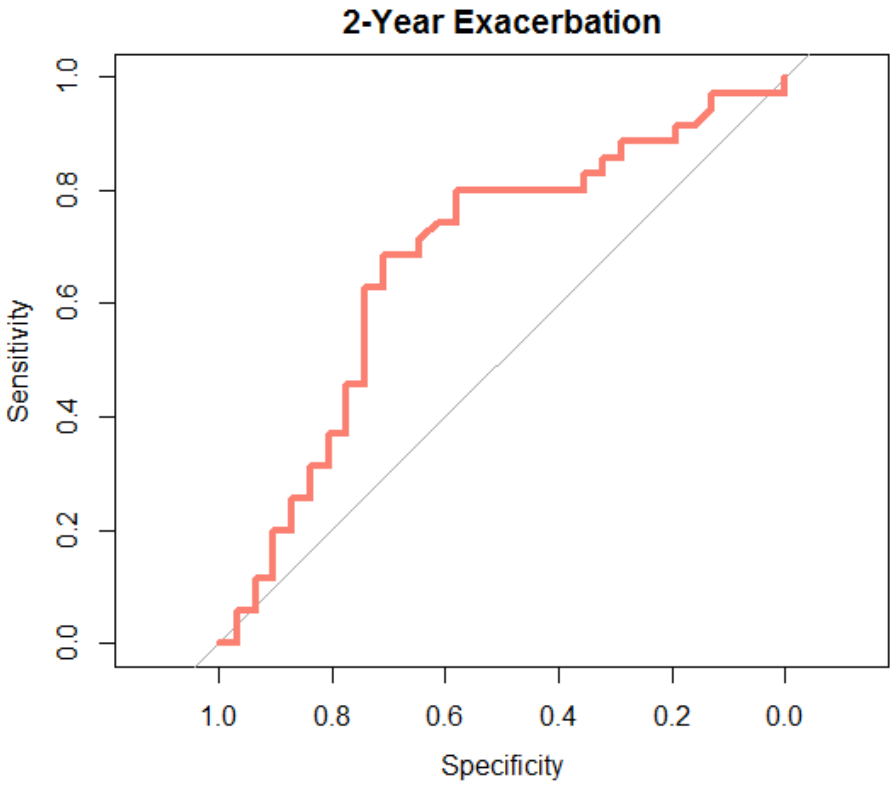

Figure 5.2. *VDP as a predictor of one or more exacerbations in the 2 years following imaging. Receiver operating characteristic (ROC) area under curve (AUC) = 0.67 (p =0.015).*

VDP was significantly associated with the presence of one or more exacerbations in the 2 years following imaging, with an ROC AUC of 0.67 (p = 0.015). No other biomarker was significantly associated with this binary indicator of prospective exacerbation (Table 5.3).

	ROC AUC	p-value
VDP	0.67	0.015
IL-6	0.67	0.068
IL-5	0.66	0.093
ACQ	0.63	0.067
FVC PP	0.61	0.11
FEV1 PP	0.61	0.11
Blood Eos	0.61	0.12
FEV1/FVC PP	0.57	0.36
Sputum Eos.	0.50	1
FeNO	0.49	0.96
ACT	0.45	0.47

Table 5.3. VDP and other biomarkers as predictors of one or more exacerbations in 2 years following imaging.

5.4.3.2 Predictor of Cumulative 2-Year Exacerbations

A VDP threshold of 4.28% was selected based on maximum likelihood estimation of the regression tree model. Subjects with VDP exceeding the threshold (N = 30) had a median [first quartile – third quartile] of 2.0 [0.25 – 3.0] exacerbations vs. 0.0 [0.0 – 1.0] for subjects below the threshold (N = 35), as shown in Figure 5.3. The exacerbation frequency ratio for subjects above vs. below the VDP threshold was 3.1 (95% CI 1.7—5.8), p=0.0007.

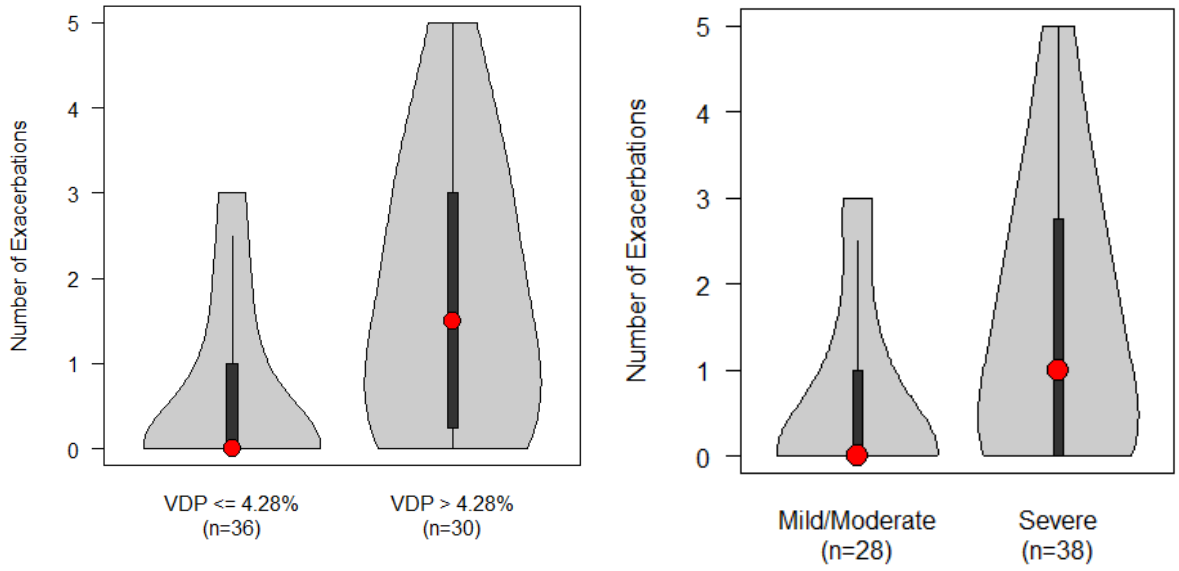

Figure 5.3: *Violin plot (left) of 2-year exacerbation frequency for subjects above and below the VDP threshold. Subjects above the threshold experienced a median of 2 exacerbations vs. zero exacerbations for subjects below the threshold (p = 0.0007). At right is the same plot stratified by asthma severity; severe subjects experienced a median of 1 exacerbations vs. zero exacerbations for mild/moderate subjects (p = 0.01).*

Table 5.4 shows the same study population stratified by the VDP threshold.

	VDP < 4.28%	VDP > 4.28%
N	35	30
Severity	23 M/M (65.7%) 12 Severe (34.3%)	5 M/M (16.6%) 25 Severe (83.3%)
Sex	16 M (45.7%) 19 F (54.3%)	11 M (36.7%) 19 F (63.3%)
Age (yrs)***	28.2 ± 16.5	48.0 ± 18.6
BMI**	24.9 ± 5.7	29.5 ± 5.9
FEV1 PP**	88.5 [82.0 – 96.4]	66.2 [53.2 – 96.0]
FEV1/FVC PP**	91.7 [87.1 – 96.3]	83.9 [77.9 – 90.8]
FVC PP***	97.5 [90.4 – 104.6]	79.3 [69.0 – 99.0]
FeNO	20.0 [9.3 – 35.3]	22.0 [13.0 – 33.0]
Blood eosinophils (counts/μL)	0.2 [0.0 – 1.1]	0.9 [0.2 – 3.6]
Sputum eosinophils (%)	184.5 [116.2 – 395.2]	272.5 [156.2 – 519.2]
ACQ**	0.71 [0.6 – 1.1]	1.3 [0.7 – 2.0]
ACT*	21.0 [19.0 – 22.8]	19.0 [15.0 – 21.0]

Table 5.4. Summary of population characteristics stratified by VDP threshold derived from predictive model. Results given as mean ± standard deviation or median [1st quartile – 3rd quartile]. All measurements acquired prior to bronchodilator administration. Significant differences indicated by * $p < 0.05$, ** $p < 0.01$, *** $p < 0.001$.

5.5 Prediction Model Incorporating History of Severe Exacerbation

In the model incorporating both recent severe exacerbation and VDP as predictors of exacerbation frequency, we found that VDP above 4.28% (p=0.0006) and prior severe exacerbation (p=0.001) were each risk factors for increased exacerbation frequency. Importantly, among subjects without a recent severe exacerbation, those with VDP above the threshold (n=18) had more frequent exacerbations than those below (n=26) (exacerbation frequency ratio = 5.6, p<0.0001), as shown in Figure 5.4.

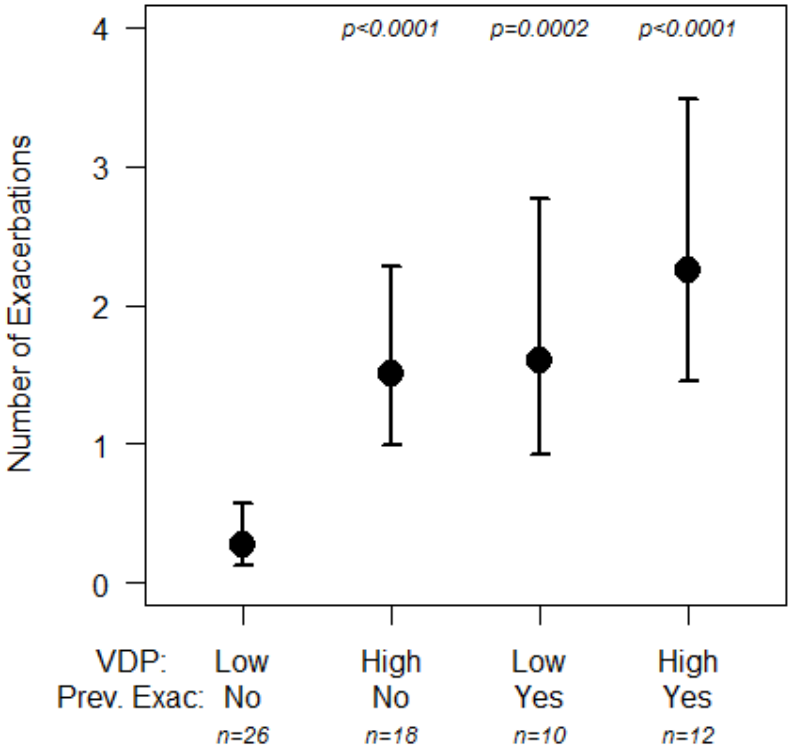

Figure 5.4. *Number of exacerbations (means with 95% CIs) stratified using VDP threshold of 4.28% (Low/High) and previous exacerbation (Yes/No) in the year prior to imaging. Subjects with history of exacerbation and/or elevated VDP had increased exacerbation frequency following imaging relative to subjects with low VDP and no history of recent exacerbation shown on the far left.*

5.6 DISCUSSION

We found that the ventilation defect percent (VDP) on hyperpolarized gas MRI is predictive of propensity for asthma exacerbation and of exacerbation frequency in the two years following imaging. This finding adds to the results of the previous section and published previously [57], which showed that VDP was associated with a history of severe exacerbation. However, this work differs from and extends that result in several key aspects. First, and most important, tracking exacerbations prospectively rather than retrospective enables an assessment of predictive value, rather than a simple association.

Second, the definition of exacerbation in this work was broadened; rather than tracking severe clinical outcomes (ED visits and hospitalizations), exacerbations were defined as any event requiring use of OCS for three consecutive days. Finally, we tracked cumulative exacerbations over a set time period of two years prospective to imaging instead of a binary indicator of exacerbation at any time prior to imaging.

In an ROC-based analysis, VDP was predictive of one or more exacerbations in the two-year period following imaging, while no other clinical measure assessed – including spirometry, blood-based measurements of cytokines and eosinophils, or survey instruments – were significant predictors, although VDP was strongly correlated with all of those measures with the exception of FeNO. This result suggests that VDP is both reflective of obstructive physiology in its conventional clinical interpretation and also sensitive to an aspect of exacerbation propensity that is opaque to other measurements. Further, we found that increased VDP was associated with increased exacerbation frequency over the two-year post-imaging period. This finding suggests that it is not only the presence but the degree of heterogenous patterns of ventilation that is associated with increased disease instability.

We also found that severe exacerbation prior to imaging was an important mediator in models of VDP as a predictor of exacerbation frequency. These results suggest that measurements of VDP in the context of exacerbation history may enable a well-defined decision-tree based approach (Figure 5.5) to monitoring treatment response both in individual subjects and in clinical trials, and for selecting patients in need of intensive therapy intervention.

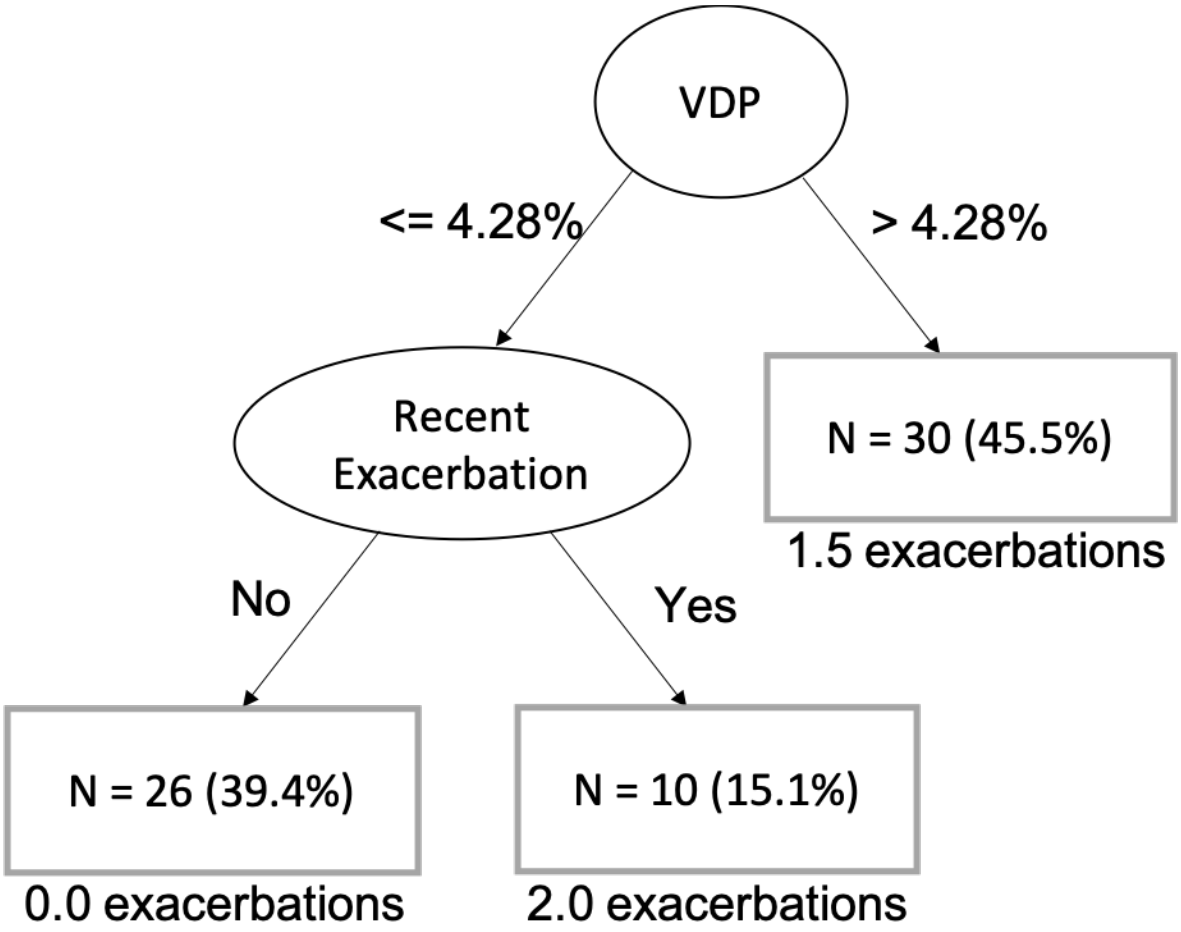

Figure 5.5. *Model-based decision tree for assessing exacerbation propensity based on history of exacerbation and VDP. Median two-year exacerbation frequency following imaging are shown for the three subgroups.*

Establishing VDP as a predictor of exacerbation frequency is useful for several reasons. As noted previously, though the cost of a HP gas MRI is currently prohibitive in most settings, it may be justified in patients with particularly severe asthma as a means of assessing suitability for costly targeted therapies (e.g. biologics such as mepolizumab or benralizumab), a topic discussed in more depth in the subsequent section. Moreover, these results suggest that VDP may have utility as a secondary endpoint in clinical trials: since reducing exacerbations is an essential component of improving quality of life in asthma, if VDP is an accepted measure of propensity for exacerbation, longitudinal

monitoring of VDP in a study population could provide an additional and possibly more accurate means of quantifying therapy response, especially in subjects with mild asthma where a severe exacerbation is relatively rare. Because the quantitative approach offered by VDP provides a means of assessing disease severity at any chosen point in time, this approach could also have utility in assessing differential responses to therapy within a study population without the need for subsequent monitoring for exacerbations over an extended period.

5.7 LIMITATIONS

The primarily limitation is that the scope of the study was not sufficient to allow for a multi-tiered assessment of exacerbation severity. A more refined scale of measuring exacerbations, or an increase in the population size and/or time scale of the study, could permit a more accurate assessment of the relationship between VDP magnitude and exacerbation severity in addition to exacerbation frequency. Replicating this study with ED visits and/or hospitalizations as the outcome was not possible since the frequency of those events was too low in a two-year period to allow for a meaningful model. However, the definition used here is presumably inclusive of both these severe events and less severe exacerbations that nonetheless required a treatment escalation (i.e. OCS). That the association between VDP and exacerbation persists after this definitional change suggests that it is sensitive to ventilation deficiencies associated with milder outcomes as well as those that require immediate emergency care. While a larger cohort and/or longer longitudinal monitoring could enable an analysis of these relatively rare events, it is reasonable to postulate from the results of these combined studies that VDP is similarly predictive of exacerbations that require emergency care.

5.8 CONCLUSION

We found that the ventilation defect percent (VDP) on hyperpolarized gas MRI is predictive of exacerbation frequency in the two years following imaging, corroborating previously published results showing that VDP was associated with a history of severe exacerbation. We also found that severe exacerbation prior to imaging was an important mediator in models of VDP as a predictor of exacerbation frequency. These results suggest that measurements of VDP in the context of exacerbation history may enable a decision-tree based approach to monitoring treatment response both in individual subjects and in clinical trials, and for selecting patients in need of intensive therapy intervention.

6 CENTRAL AIRWAY MUCUS PLUGGING ON CT IS ASSOCIATED WITH VENTILATION HETEROGENEITY ON HYPERPOLARIZED GAS MRI IN ASTHMA

6.1 ABSTRACT

6.1.1 Purpose.

Mucus hypersecretion has been associated with decreased lung function and severe exacerbation in asthma, but its direct impact on ventilation heterogeneity has yet to be studied. Hyperpolarized helium-3 magnetic resonance imaging (HP ^{3}He MRI) enables assessment of the functional abnormalities associated with airway mucus plugging observed on CT. We test the hypothesis that mucus hypersecretion is a driver of ventilation heterogeneity in asthma by evaluating regional correlations between mucus plugs on CT and the VDP on HP ^{3}He MRI.

6.1.2 Methods

Mucus plugs were scored by lobe on CT for 33 asthma subjects, all of whom also underwent HP ^{3}He MRI to determine lobar VDP. Mucus plugs and VDP were assessed for each individual bronchopulmonary segment in a subset of 8 subjects due to the time-intensive nature of the analysis. We assessed correlations between mucus plugs and associated regional measures of VDP.

6.1.3 Measurements and Main Results

Mucus plug score was correlated with increased VDP in the whole lung (Spearman's r = 0.65, p < 0.0001) and by lobe (RUL: r=0.64, p<0.001; RML: r=0.42, p=0.019; RLL: r=0.63, p<0.001; LUL: r=0.51, p<0.01; LLL: r=0.38, p=0.035). Bronchopulmonary segments with a positive mucus plug score had significantly increased VDP (p < 0.0001). The relative risk of a ventilation defect in segments with a positive mucus score was 1.91.

6.1.4 Conclusions

Mucus plugging on CT was associated with reduced lobar and segmental ventilation on HP ^{3}He MRI, suggesting that mucus plugging is associated with ventilation heterogeneity observed on HP ^{3}He MRI in asthma.

6.2 INTRODUCTION

Ventilation heterogeneity, the non-uniform distribution of inspired gas within the lung, is a ubiquitous feature of asthma and is revealed in the ventilation defects observed on hyperpolarized helium-3 gas magnetic resonance imaging (HP ^{3}He MRI) [59, 60]. These defects are associated with a history of severe exacerbation [57], with local increases in neutrophils [26], and with air trapping and airway wall thickening [26, 61] on computed tomography (CT). Mucus hypersecretion in asthma has long been associated with inflammation and injury of the airway and with severe exacerbations in asthma [62-64]. Focal regions of increased mucus secretion ("mucus plugs") can be visualized on CT and have been associated with eosinophilia and reduced lung function as measured on spirometry [14]. Despite the implication of mucus plugging as a source of reduced lung function and severe outcomes, to our knowledge no study has yet assessed regional correlations of mucus plugging in asthma with regions of poor ventilation ("ventilation defects") observed on HP ^{3}He MRI.

To test the hypothesis that mucus plugs are a cause of ventilation defects in asthma, we evaluate global and regional correlations between mucus plugs on CT and the associated ventilation defect percent (VDP) on HP ^{3}He MRI.

6.3 METHODS

Subjects in this study were drawn from the "Longitudinal" population described in Section 3.2, restricted to subjects with both regional measures VDP and mucus plugs identified on CT. Differences in quantitative variables between the mild/moderate and severe asthma groups as defined by the SARP criteria [7].

All subjects underwent spirometry after administration of four puffs of albuterol, a β-agonist bronchodilator (BD). Blood analysis and measurements of FeNO were performed as described previously [7]. Percent predicted (PP) values for forced expiratory volume in one second (FEV_1), forced vital capacity (FVC), and FEV_1/FVC were generated using the Global Lung Function Initiative reference values [46].

6.3.1 Image Analysis

Mucus plug scoring was performed on CT by two radiologists with 2 years of experience using the scoring system developed by Dunican et al. [14]. Mucus plug scores were assessed by lobe and aggregated into whole lung scores, with the reader scores averaged by lobe in case of a disagreement. A binary mucus plug score recorded as present or absent was determined for each bronchopulmonary segment in only a subset of the full study population due to the labor-intensive nature of determining the specific anatomical location of mucus plugs. Example images of a mucus plug visualized on CT and a spatially overlapping ventilation defect on HP ^{3}He MRI are shown in Figure 6.1, and an overview of the study population and procedures is shown in Table 6.1.

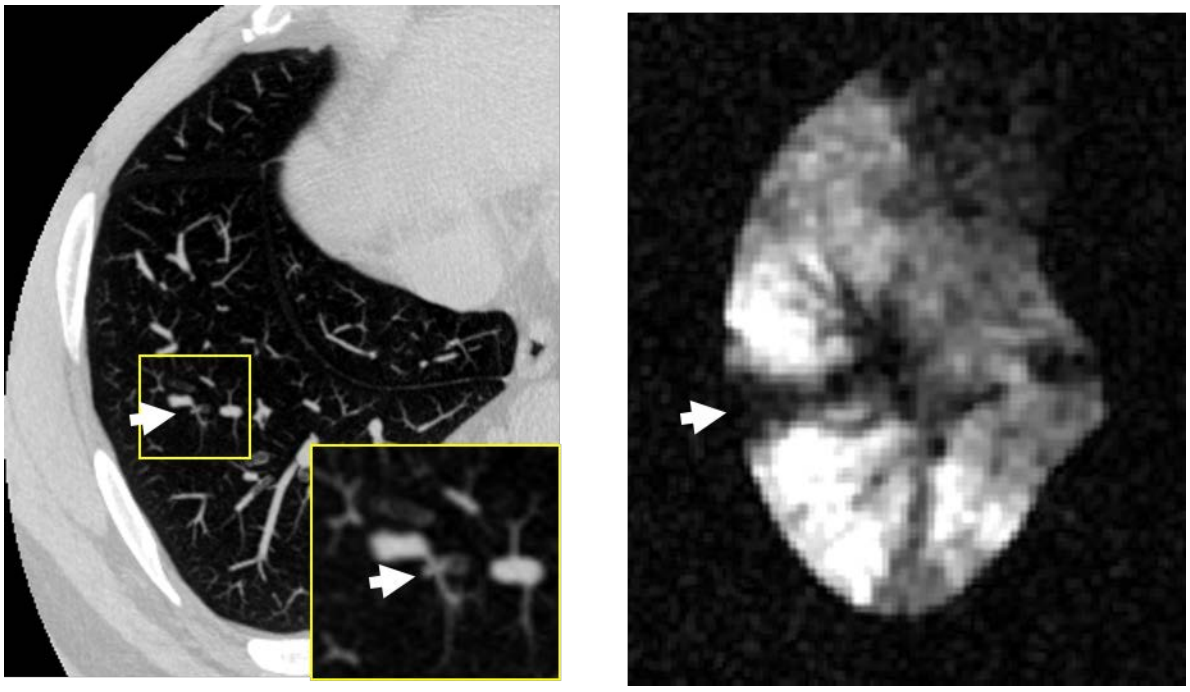

Figure 6.1*. Example images of a mucus plug (arrow) visualized on CT (left) and a spatially overlapping ventilation defect (arrow) on HP ^{3}He MRI (right). Inset on left shows close-up of mucus plug (arrow). Inset is a maximum intensity projection (3.15 mm) at the level of the mucus plug.*

Image Acquisition and Processing Stages	N (%)
1. Total SARPIII population at UW-Madison	107 (100%)
↳ 2. Subjects undergoing inspiratory CT	78 (72.9%)
↳ 3. CT scored for mucus plugs	41 (38.3%)
↳ 4. **With corresponding HP ^{3}He MRI**	**31 (29.0%)**
↳ 5. **Substudy:** Segmental mucus plug and HP ^{3}He MRI	8 (7.5%)

Table 6.1. Study population and image processing steps with number and percent of total at each stage. The primary analysis population (CT scored for mucus plugs together with corresponding HP ^{3}He MRI) is shown in Stage 4; the substudy using segmental mucus plug scores is shown in Stage 5.

CT images were processed through VIDA Diagnostics software (VIDA Diagnostics, Coralville, IA) to generate a lobar and segmental anatomical mask. The HP ^{3}He MRI lung boundary was segmented with reference to proton MRI using in-house software written in MATLAB (The MathWorks, Natick, MA). The CT lung boundary mask from VIDA was

deformably registered to the HP ^{3}He MRI boundary mask using the ANTs software package (http://stnava.github.io/ANTs/), and the resulting transformation was applied to the original CT images and anatomical mask, thereby registering them to the HP ^{3}He MRI (see image analysis workflow in Figure 6.2).

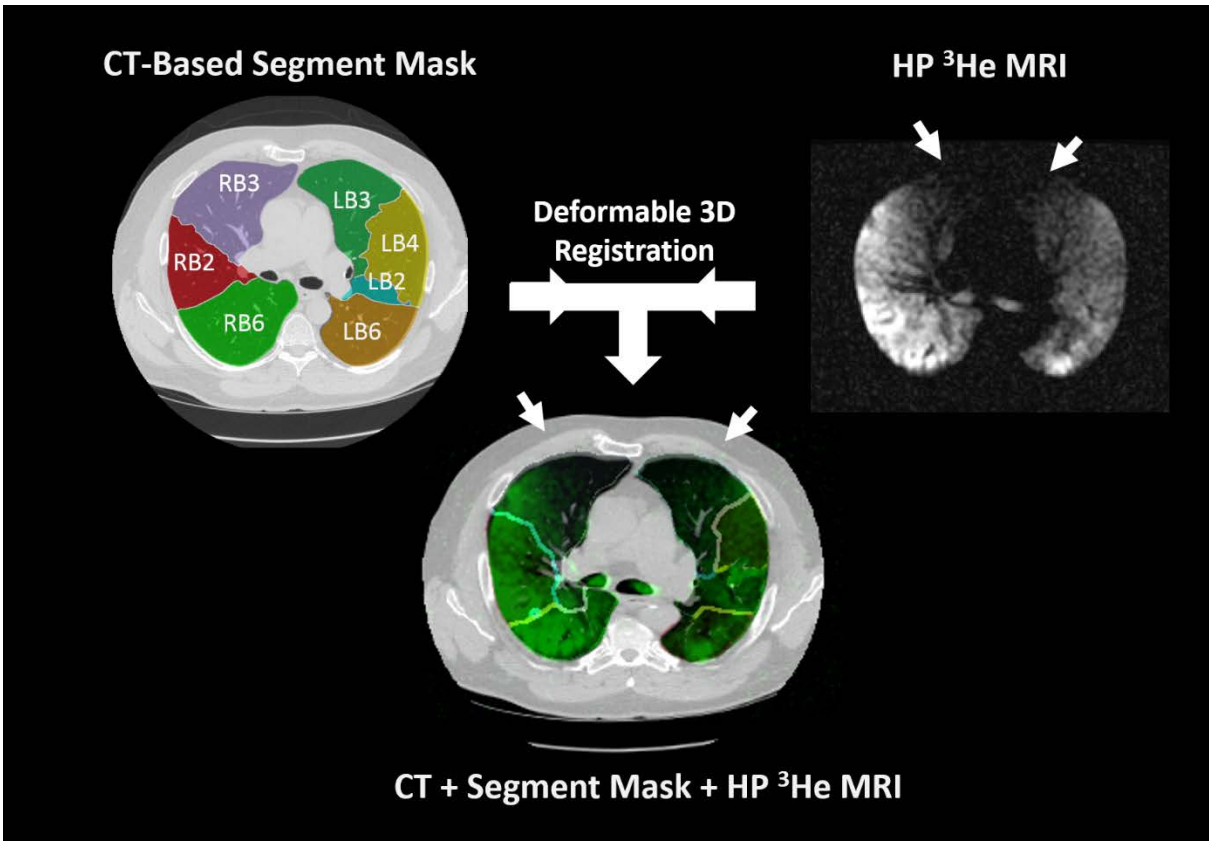

Figure 6.2. *Top row shows bronchopulmonary segment mask with CT and ventilation image on HP ^{3}He MRI. The CT and segment mask are registered to the HP ^{3}MRI to calculate the segmental ventilation defect percent (SVDP, bottom).*

Ventilation defects were classified on HP ^{3}He MRI using a semi-automated algorithm [58] to calculate whole-lung VDP. Lobar VDP and VDP by individual bronchopulmonary segment (segmental VDP or SVDP) were determined using the CT segmental mask generated by VIDA registered to the whole lung ventilation defect mask,

a method based on the technique described by Thomen et al. [28]. For each bronchopulmonary segment, a binary “defect score” analogous to the CT mucus score was derived using an SVDP threshold of 5.0%.

6.3.2 Statistical Methods

Differences in quantitative variables between the mild/moderate and severe asthma groups were assessed using the Wilcoxon rank-sum test. Correlations between whole lung/lobar VDP and corresponding mucus plug scores were assessed using the Spearman rank correlation. In the subpopulation with binary mucus plug scores by bronchopulmonary segment, we used two methods to assess differences in ventilation in the presence of a mucus plug: differences in absolute SVDP assessed using the Wilcoxon rank-sum test, and the relative risk associated with a defect (i.e. SVDP > 5.0%) assessed using Wald-based confidence intervals and Fisher’s exact test. A p-value of 0.05 was used for the threshold of statistical significance. Statistical analyses were performed using R version 3.2.3 (https://www.r-project.org/).

6.4 RESULTS

6.4.1 Study Population

Study population characteristics are summarized in Table 6.2, and include subjects with mild/moderate (N = 12, 38.7%) and severe (N = 19, 61.2%) asthma. BMI, plasma IL-5 and IL-6, and VDP were significantly increased in the severe vs. mild/moderate group; FEV1 PP and FVC PP were significantly reduced.

	Mild/Moderate	Severe	All
N	12	19	31
Sex	7F (58.3%)	12 F (63.1%)	19F (61.3%)
Age	44.5 ± 16.2 yrs	56.3 ± 9.9 yrs	51.8 ± 13.7 yrs
BMI*	27.4 ± 5.6	32.0 ± 5.3	30.2 ± 5.8
FEV1 PP*	88.3 [73.2 – 105.1]	75.6 [62.9 – 94.1]	83.2 [71.3 – 100.5]
FEV1/FVC PP	97.9 [90.1 – 101.1]	90.0 [65.4 – 98.5[	95.2 [84.3 – 108.9]
FVC PP *	102.0 [92.9 – 106.0]	85.7 [77.0 – 94.6]	89.8]84.3 – 103.7]
FeNO	24.0 [16.0 – 33.0]	14.0 [10.2 – 22.8]	19 [11.5 – 31.0]
Blood eosinophils (counts/μL)	189.0 [106.0 – 250.0]	237.0 [147.5 – 374.0]	221.5 [134.5 – 303.8]
Sputum eosinophils (%)	0.4 [0.0 – 1.0]	0.6 [0.3 – 2.1]	0.6 [0.0 – 1.6]
Plasma IL5*	15.8 [15.3 – 17.7]	19.4 [17.8 – 20.3]	18.0 [15.8 – 19.5]
Plasma IL6*	1.0 [0.7 – 1.3]	1.6 [1.2 – 2.3]	1.3 [0.9 – 1.9]
CT Mucus Score	0.0 [0.00 – 0.5]	0.25 [0.0 – 8.2]	0.0 [0.0 – 2.0]
VDP (%)*	4.6 [1.1 – 4.6]	5.6 [3.4 – 12.3]	4.1 [2.5 – 10.4]

Table 6.2. Summary of population characteristics. Results given as mean ± standard deviation or median [1st quartile – 3rd quartile]. Spirometry percent predicted (PP) is shown after bronchodilator to match imaging protocol. Mucus score and VDP reported here are whole-lung. Differences in quantitative values between mild/moderate and severe groups were assessed using the Wilcoxon rank sum test. * $p < 0.05$, ** $p < 0.01$.

6.4.2 Global Comparisons

FEV_1 PP and FEV_1/FVC PP were both negatively correlated with aggregate whole lung mucus plug score ($r = -0.40$, $p = 0.021$ and $r = -0.46$, $p < 0.01$ respectively) and with whole lung VDP ($r = -0.51$, $p = 0.0046$ and $r = -0.51$, $p = 0.0046$ respectively). FVC PP was not correlated with whole lung mucus score or VDP.

Whole lung VDP was correlated with whole lung mucus score ($r = 0.65$, $p < 0.0001$) as illustrated in Figure 6.3.

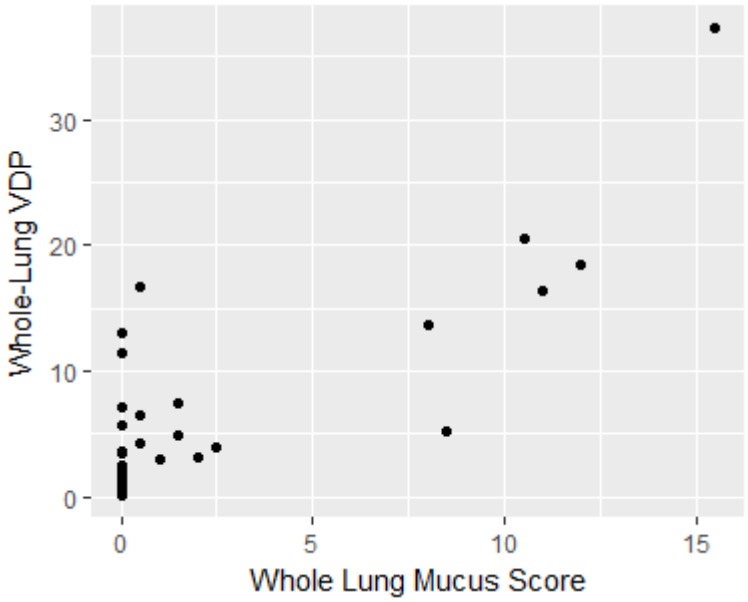

Figure 6.3. *Whole-lung mucus score vs. whole-lung VDP. Spearman's correlation is 0.65 ($p < 0.0001$).*

Whole-lung VDP was not correlated with sputum eosinophil differential, blood eosinophil counts, plasma IL-5, or plasma IL-6. Mucus plug scores were positively correlated with sputum eosinophil differential ($r = 0.57$, $p = 0.0015$) but not with blood eosinophil counts, plasma IL-5, or plasma IL-6, although the correlation with IL-5 was on the cusp of significance ($r = 0.43$, $p = 0.05$).

6.4.3 Regional Comparisons

Lobar VDP was significantly correlated to lobar mucus score in all 5 lobes as shown in Figure 6.4 (RUL: $r = 0.64$, $p < 0.001$; RML: $r = 0.42$, $p = 0.019$; RLL: $r = 0.63$, $p < 0.001$; LUL: $r = 0.51$, $p < 0.01$; LLL: $r = 0.38$, $p = 0.035$).

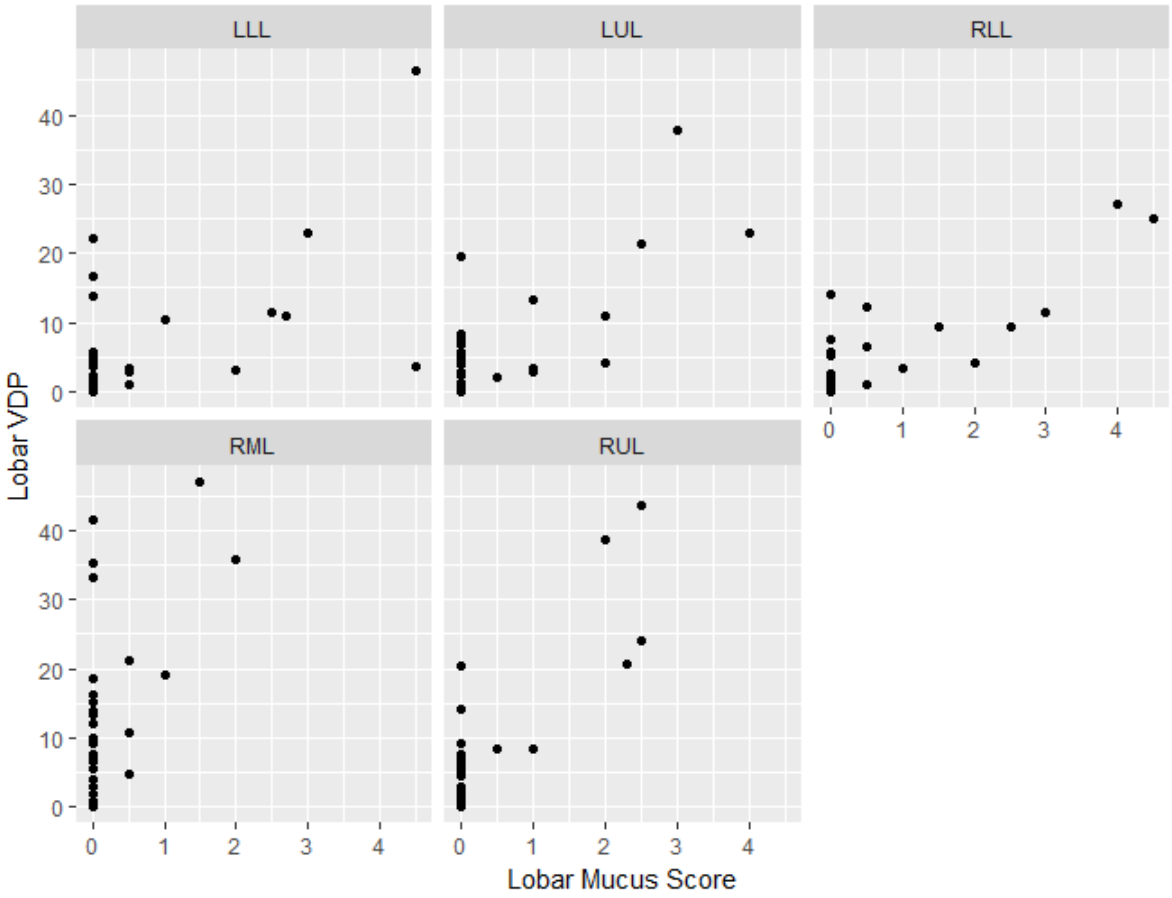

Figure 6.4 *Lobar mucus score vs. lobar VDP. Spearman's r (p-value) by lobe: RUL, r = 0.64 (p < 0.001); RML, r = 0.42 (p = 0.019); RLL, r = 0.63 (p < 0.001); LUL, r = 0.51 (p < 0.01), r = 0.38 (p = 0.035).*

Binary mucus plug scores were assessed by individual bronchopulmonary segment in a subset of 8 subjects, resulting in measurements for 8 x 19 = 152 total segments, of which 59 (38.8%) had a mucus plug. In segments with a mucus plug the median [1Q – 3Q] SVDP was 9.4% [3.6% - 28.5%] vs. 3.2% [0.4% - 7.8%] in segments without a plug ($p < 0.0001$), as shown in Figure 6.5.

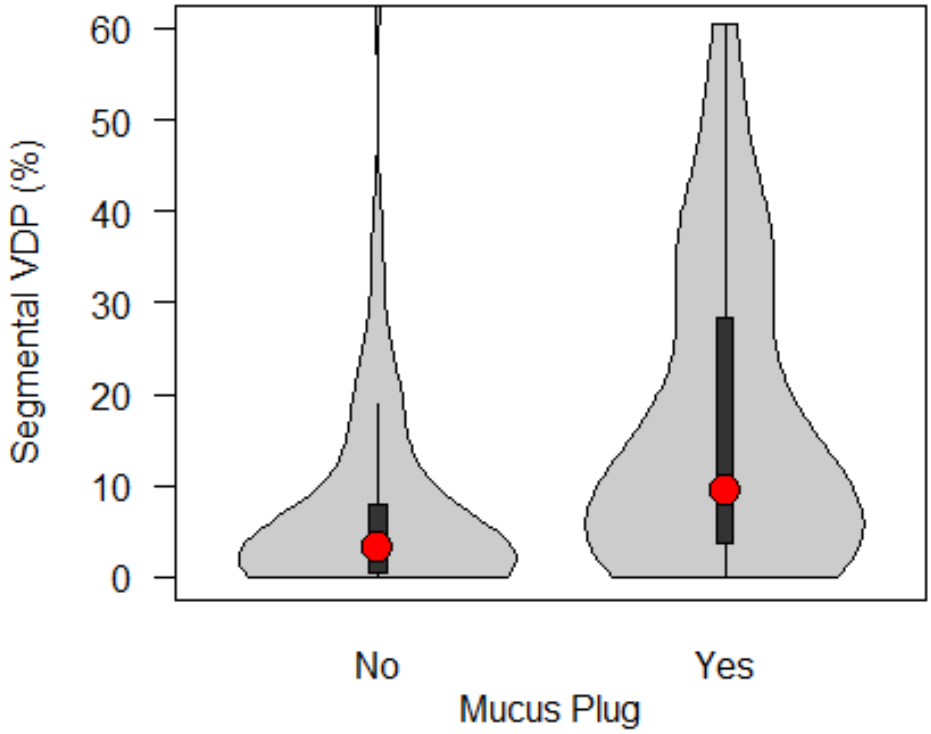

Figure 6.5. *Violin plot of segmental ventilation defect percent (SVDP) vs. binary mucus plug score. SVDP in segments with a mucus plug was median [1Q – 3Q] of 9.4% [3.6% - 28.5%] vs. 3.2% [0.4% - 7.8%] in segments without ($p < 0.0001$).*

Ventilation defects (SVDP > 5.0%) were detected in 40/59 (67.8%) of segments with a mucus plug vs. 33/93 (35.5%) of segments without a mucus plug, resulting in a relative risk of a ventilation defect in segments with a positive mucus score of 1.91 (95% CI 1.38–2.65, p=0.0001).

6.5 DISCUSSION

Mucus hypersecretion is a common feature of asthma, particularly in relation to exacerbations [62] and in subjects who have died of status asthmaticus [64]. We found that CT-based measures of localized mucus hypersecretion (“mucus plugs”) were associated with regions of poor ventilation (“ventilation defects”) measured on

hyperpolarized helium gas MRI. This relationship held true in the whole lung, by lobe, and by bronchopulmonary segment, with a mucus plugged bronchopulmonary segment having almost twice the risk of a ventilation defect vs. a plug-free segment. These results provide the first evidence that focal areas of mucus hypersecretion in asthma drive a significant fraction of regional ventilation defects in asthma, building on previous work [14] showing that mucus plugging was associated with reduced whole lung pulmonary function on spirometry.

With a diverse range of targeted, but costly, therapeutic asthma drugs on the horizon, there is a growing need for techniques that can be used to select asthma patients for specific therapies and to monitor and evaluate treatment response. Mucus plugs have been associated with eosinophilia [14], indicating a role in reducing mucus-related obstruction for monoclonal antibodies that inhibit IL-5 (a cytokine associated with eosinophil activity) such as mepolizumab [65] and reslizumab [66], as well as for benralizumab [67], which depletes blood and airway eosinophils. Multiple drugs that specifically target goblet cell hyperplasia have also been proposed for use in asthma, including simvastatin [68] and ellagic acid [69], both of which have shown efficacy in mice models. An imaging technique capable of evaluating airway obstruction related to mucus plugs could thus prove useful in developing and testing targeted therapies, informing clinical decision making, and evaluating response on a patient-by-patient basis, particularly in severe cases where the high cost of therapy and/or a severe clinical outcome could justify the cost of an advanced imaging exam.

It is important to note that at all lung volumes under consideration, ventilation defects were not always associated with mucus plugging – on the order of 35% of the

time in individual bronchopulmonary segments. Though imaging was acquired post-bronchodilator to minimize effects of airway hyperresponsiveness, and though it is certainly possible that there are mucus plugs beyond the resolution of CT, it is nonetheless likely that factors other than mucus plugging are also associated with ventilation defects in asthma as suggested by Svenningsen et al. [25]. The methodology presented here could be used to investigate the functional significance of these other measures of ventilation and airway obstruction on a regional basis, such as functional small airways disease [70], smooth muscle hyperresponsiveness [71, 72], airway wall thickness [25], and localized (i.e. voxel-based) measures of ventilation heterogeneity [73]. In addition, these regional assessments could be complemented by additional models of ventilation heterogeneity assessed by models of pendelluft [74] and patient-specific simulations of gas flow (Oakes *IEEE Trans Biomed Eng.* 2018 [In Press])**,** impulse oscillometry [75], and multiple-breath nitrogen washout [60]. Simultaneous evaluation of multiple biomarkers of obstruction under this paradigm could advance efforts towards a more holistic understanding of those biomarkers' associations with, and potential causation of, ventilation heterogeneity. This knowledge may prove useful not only in advancing knowledge of specific disease mechanisms, but also in the characterization of imaging-based phenotypes and could be used to guide the development and administration of targeted therapies and to underpin a multi-pronged approach to monitoring therapy response and disease progression.

6.6 LIMITATIONS

There are limitations to this work. First, there are only a small number of subjects with mucus plugs scored by bronchopulmonary segment, due in part to the highly labor-

intensive task of visually identifying and anatomically locating the mucus plugs on CT. Thus, the apparent segmental association between mucus plugs and SVDP could be driven by subjects who have uniformly high (or low) levels of both mucus plugs and ventilation defects across their entire lung. However, the lobar correlations in the full study population suggest at a minimum that the observed segmental associations are plausible and warrant further scrutiny in a larger population. Second, this method of CT mucus scoring does not discriminate mucus extent beyond the level of the bronchopulmonary segment, instead reducing it to a single binary indicator. Future efforts to develop an automated scoring algorithm could help refine, streamline, and standardize the counting process, thereby enabling analysis at an additional level of detail and in a larger population.

6.7 Conclusion

This study establishes that mucus plugging is associated with the regional ventilation defects that are characteristic of asthma. The approach presented here enables a comprehensive evaluation of the functional significance of localized biomarkers of airway limitation and obstruction in the framework of lobar and segmental measures of ventilation on hyperpolarized gas MRI. Future work could employ an assessment of these and other such regional biomarkers towards the evaluation of targeted therapeutic agents aimed at specific drivers of ventilation heterogeneity in obstructive lung disease.

7 IMAGE-GUIDED BRONCHOSCOPY

7.1 INTRODUCTION

Asthma exhibits considerable heterogeneity both across patients and within the lungs of individual asthmatics. Multiple frameworks have been proposed for characterizing asthma phenotypes, including those based on overall severity [7], specific symptoms and measures of inflammation [76], eosinophilia [77], and phenotypes specific to children [78].

Ventilation defects on HP ^{3}He MRI in asthma have been associated with localized air trapping [26], elevated levels of neutrophils on bronchoalveolar lavage (BAL) [26], and airway wall thickness [25]. VDP has been shown to reflect changes in ventilation after bronchial thermoplasty [28], and high levels of sputum eosinophils have been correlated with reduced bronchodilator response as measured by the change in VDP [79]. However, a comprehensive analysis of cellular activity in regions of airway obstruction as identified regionally on imaging has yet to be conducted.

BAL cell counts and histochemical and immunohistochemical stains of biopsies obtained via endotracheal bronchoscopy enable regional measures of cellular activity and inflammatory response, and investigative bronchoscopy has been shown to be well tolerated in a large population of asthmatic subjects [80]. In this work, bronchoscopy was guided prospectively using CT and HP MRI to obtain paired samples from regions of ventilation defect and well-ventilated control sites within the same subject. We analyze localized cellular activity on BAL and on biopsy samples stained with a suite of structural, histochemical, and immunohistochemical markers in a pilot study of subjects who have a

history of viral-induced asthma exacerbation. This *ex nihilo* pipeline for image-guided bronchoscopic sampling and analysis enables a comprehensive and quantifiable assessment of variations in cellular activity associated with regional measures of airway obstruction on HP MRI.

7.2 METHODS

7.2.1 Population

Study subjects were drawn from the “Retrospective” population described in Section 3.1. BAL samples from ten subjects who underwent bronchoscopy of both a poorly-ventilated and a control site were assessed. A subset of four of these subjects were select for staining and analysis of tissue biopsies based on quality of the biopsy sample. Bronchoscopy was performed 6-8 weeks following imaging

7.2.2 Bronchoscopic Image Guidance

Regions of poor ventilation and well-ventilated control sites were identified prospectively on either HP ^{3}He MRI or CT. For the MR-based analysis, ventilation defects were visually identified on an axial slice of the HP MRI image and located anatomically using the corresponding slice from a proton MRI or CT image as a reference. The locations of the target and control sites were then conveyed to the bronchoscopist for sampling (see Figure 7.1).

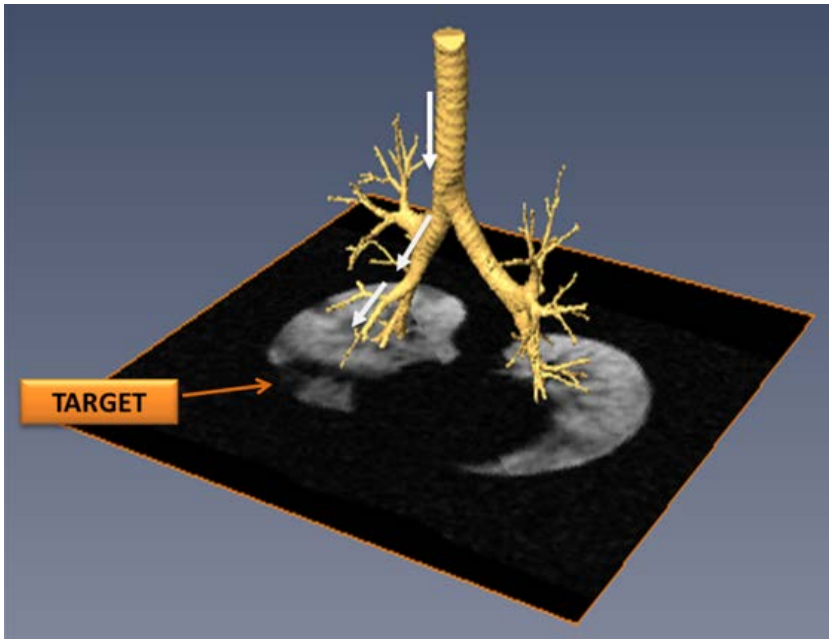

Figure 7.1. *Illustration of 3D airway tree generated from CT (VIDA Diagnostics, Coralville, IA) superposed on axial hyperpolarized gas image. An example path through the airway tree towards area of ventilation defect ("target") is shown*.

7.2.3 Bronchoscopy

Ten subjects with paired target and control sites underwent targeted endobronchial biopsy. BAL samples and tissue biopsies were obtained, and biopsy samples were embedded in paraffin and frozen before being sectioned and mounted on slides. BAL samples were analyzed for all ten subjects. Hematoxylin and eosin (H&E) stains were performed on biopsy samples and a subset of four subjects were selected for further histochemical (HC) and immunohistochemical (IHC) staining based on visual evaluation of the H&E stains by an expert pathologist to ensure sample quality.

7.2.4 Biopsy Staining

In addition to H&E staining, the HC/IHC stains shown in Table 7.1 were performed on the paired samples from the selected subset of four subjects.

Stain	Primarily Indicates …
CD4	T-helper cells, monocytes, macrophages
CD8	Cytotoxic T-cells
CD10	Mature granulocytes
CD20	B-cells
CD68	Monocytes and macrophages
CD117	Mast cells
CD138	Cell proliferation
Ki-67	Cell proliferation
Synaptophysin	Neuroendocrine cells
Trichrome	Connective tissue, nuclei, and cytoplasm
Alcian Blue/PAS	Mucus

Table 7.1. Stains performed on paired biopsy samples.

Slides were digitized at 20x magnification.

7.2.5 Digitized Biopsy Analysis

Image-based analysis of biopsy samples was performed using Aperio ImageScope software (https://www.leicabiosystems.com/digital-pathology/manage/aperio-imagescope/). Measurements of basement membrane thickness were performed on the H&E stains in the full population of ten subjects using ImageJ software (https://imagej.nih.gov/ij/). Measurements were obtained in regions with intact epithelium and in regions denuded of epithelium (Figure 7.2).

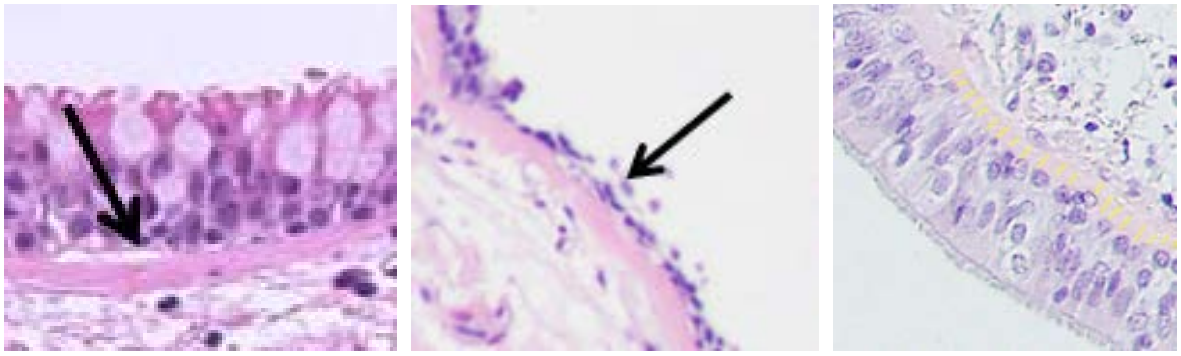

Figure 7.2. *Illustration of methodology for performing basement membrane thickness measurements on H&E scans in regions of intact epithelium (left) and with denuded epithelium (center). Approximately 20 transverse membrane thickness measurements were averaged for each data point (right).*

Regions of interest (ROI's) of a standard size were defined on H&E stains for each sample by an expert pathologist both in regions of epithelium and in regions deep to the epithelium. These ROI's were transferred to equivalent areas in the adjacent HC/IHC-stained slides by the scientist performing image-based measurements followed by manual counts of stained cells in the epithelial and non-epithelial ROI's (Figure 7.3). Counts were normalized to total ROI area for subsequent comparison.

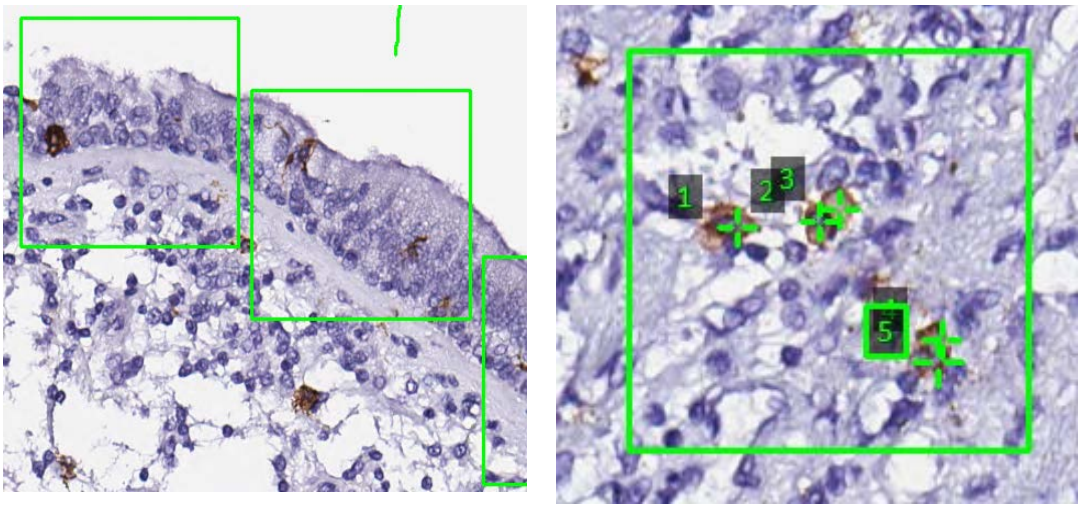

***Figure 7.3**. Example regions of interest (ROI's) defined on epithelium (left) an individual ROI with individual cells counted in a region deep to the epithelium (right).*

7.2.6 Statistical Analysis

Differences in cell counts on BAL samples between paired target and control sites were assessed using a Wilcoxon signed-rank test.

7.3 RESULTS

7.3.1 Bronchoalveolar Lavage

Total granulocytes (eosinophils + neutrophils) were significantly increased in paired measurements in sites of ventilation defect vs. well-ventilated control sites within the same subject ($p < 0.05$, Figure 7.4).

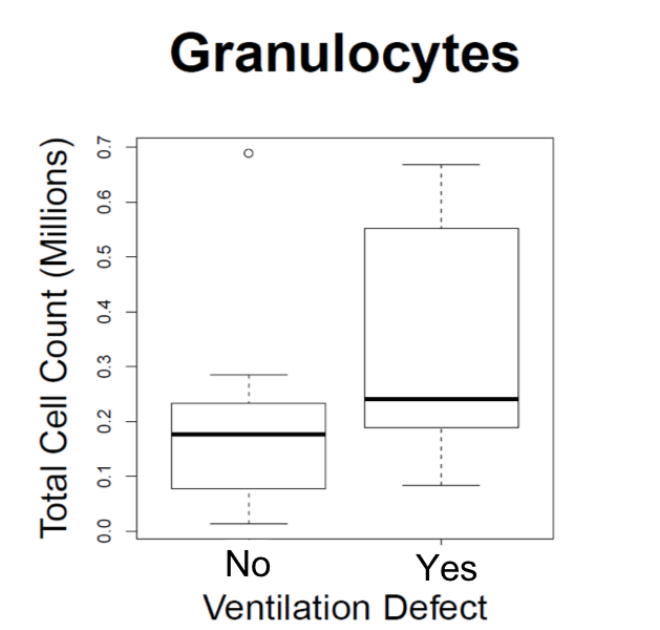

Figure 7.4. *Total granulocytes were significantly increased in sites of ventilation defect vs. a well-ventilated control site within the same subject ($p < 0.05$).*

7.3.2 Image-Guided Biopsy

Descriptive characteristics of the four-subject population subset designated for biopsy are shown in Table 7.2.

Subject	Age	Sex	FEV1 PP	FEV1/FVC PP	NLF
42	18	M	106%	94%	RSVB, CV
96	23	M	94%	100%	RV
110	26	F	84%	76%	RV
126	26	F	120%	105%	RV

Table 7.2. Descriptive characteristics of the four-subject population subset designated for biopsy. NLF – nasal lavage fluid; RSVB – respiratory syncytial virus B; CV – coronavirus; RV – rhinovirus.

Paired example images from ventilation defect vs. control sites for CD4, Trichrome, and Periodic Acid-Schiff (PAS) stains are shown in Figure 7.5 showing qualitative evidence

of increased CD4 (top row), squamous metaplasia (middle row), and goblet cells/mucin (bottom row).

Stain	Defect Site	Control Site
CD4	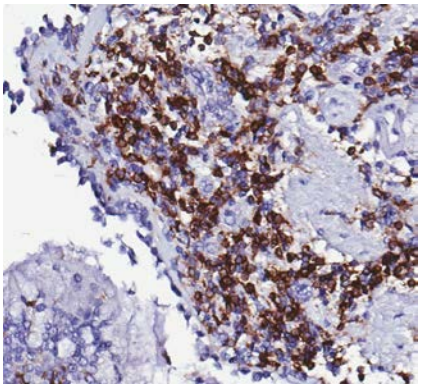	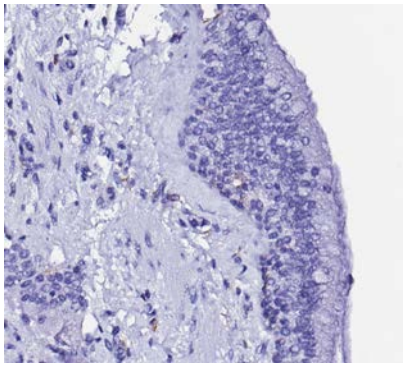
Trichrome	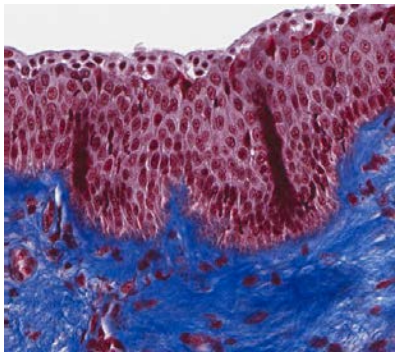	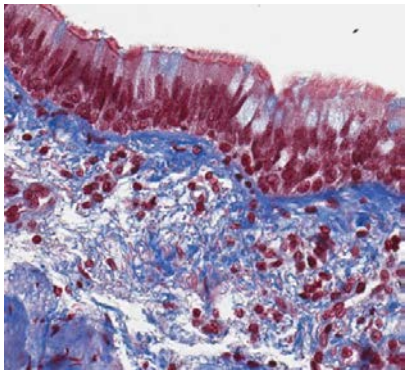
PAS	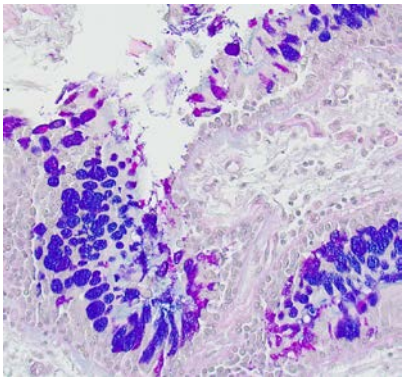	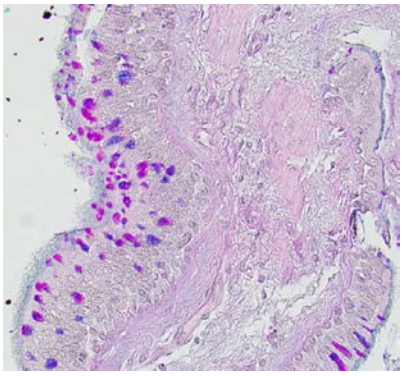

Figure 7.5*. Image-guided biopsy samples from defect (left) and control (right). CD4 stain (top row) shows increased inflammatory response in defect. Trichrome (middle row) shows increase collagen in blue indicative of fibrosis, and squamous cell metaplasia in epithelium vs. columnar, ciliated epithelium in control site. Periodic Acid-Schiff (PAS, bottom).*

Paired cell counts for each ROI for each subject & stain are showed in Figure 7.6, with median counts values connected by a line. Differences in median cell counts in defect vs. control sites for each stain were not significant in this small pilot population.

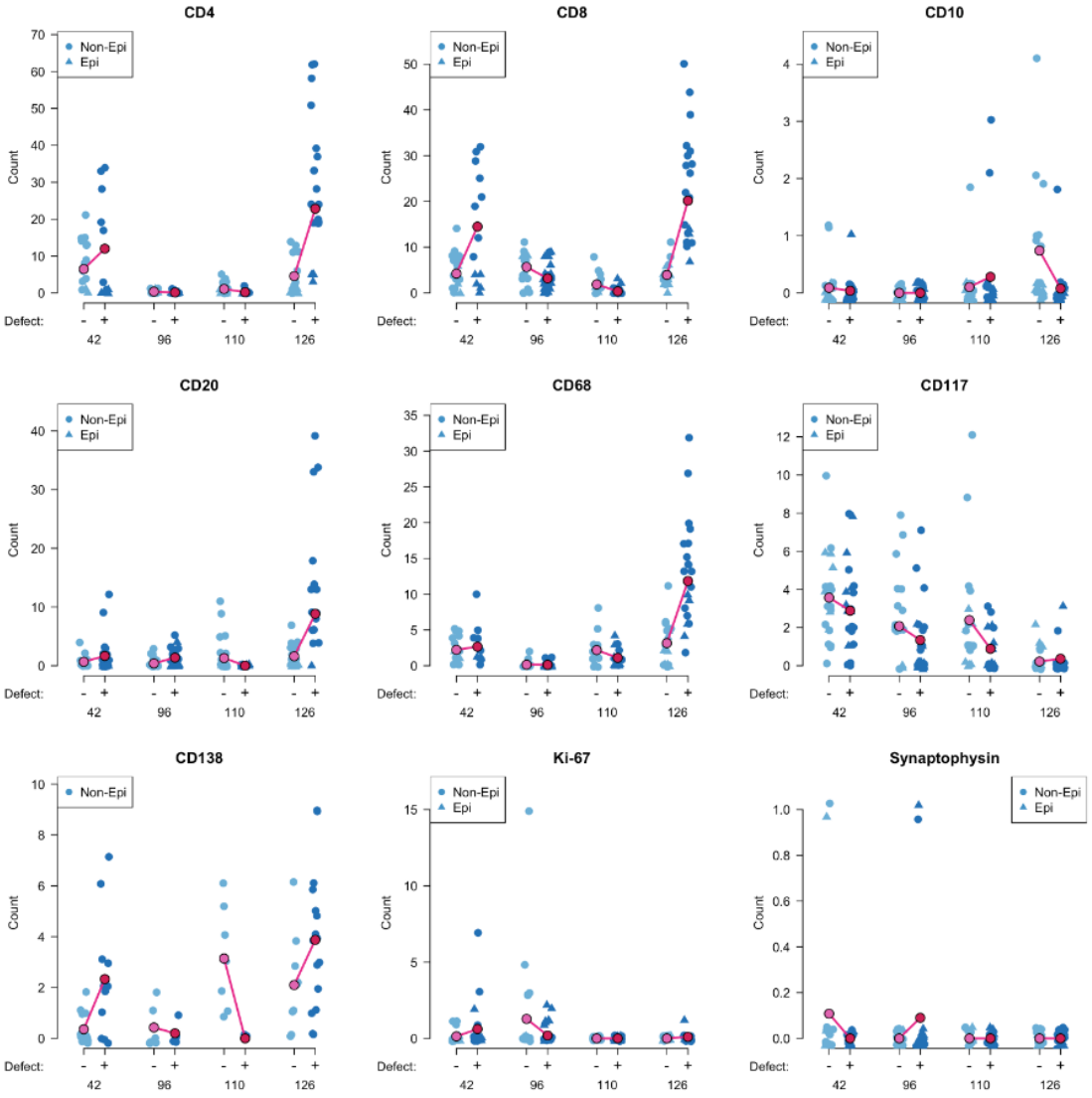

Figure 7.6. *Cell counts displayed across 9 stains, with paired defect/control sites indicated by the plus and minus signs respectively. Lines connect median values of cell counts in defect vs. control sites. Counts from regions of interest in epithelium indicated by triangles, and from regions deep to the epithelium indicated by circles*

7.4 DISCUSSION

By using HP gas MRI to guide bronchoscopic assessment of airway morphology and cellular activity in asthma, this work provides a means of bridging the gap between studies of ventilation defects and studies of the inflammatory characteristics of asthma. By using ventilation imaging to inform targeted sampling, the methodology and pipeline that we have developed here provides a means of assessing regional, localized associations between direct measurements of biomarkers of inflammation and obstruction and their functional significance on the HP gas image, adding multiple levels of granularity to the context of these invasive measurements and increasing confidence in interpretation of observed associations with impaired ventilation.

We observed that overall granulocytes, here defined as eosinophils plus neutrophils, on image-guided BAL were significantly increased in sites of ventilation defect vs. well-ventilated control sites in a population of 10 asthmatic subjects, adding a regional element to previous studies [26] indicating that ventilation defect extent was associated with increased levels of neutrophils. This suggests a localized element to the inflammation associated with airway obstruction, and that further studies of BAL cell counts localized to target sites may provide insights into cellular activity underlying airway obstruction that are opaque to whole-lung measures such as eosinophil/neutrophil levels in blood or sputum.

We then conducted analysis of image-guided biopsy samples. First, we performed measurements of airway wall thickness in paired defect vs. well-ventilation control sites, but did not observe significant differences. However, there are many outside factors that could influence this result, chiefly, inherent regional variations in lung morphology, but

also the difficulty in obtaining a bronchoscopy sample at a consistent level of branching down the airway tree. Combine these factors with the dependence of measurements on having a transverse biopsy – any degree of obliquity would affect the result – and it is not surprising that we were unable to detect differences in airway wall thickness in this small population of asthmatics. Thus, these preliminary findings are insufficient to call into question previous work associating airway wall thickness with regional ventilation defects.

Second, in a subpopulation of 4 subjects we conducted a pilot study of a pipeline for staining image-guided biopsy samples with a suite of histochemical and immunohistochemical markers of airway injury, cellular proliferation, and inflammatory response. While our sample size was insufficient to draw any statistically significant conclusions, we did observe clear visual differences on defect vs. control sites in multiple subjects, as shown in Figure 7.5. Quantitative analysis suggested heterogenous results across subjects; one subject in particular (Subject 126 in Figure 7.6) showed a marked increase in median counts across multiple stains.

A major element of this work was the creation of the “imaging to cell counts” workflow, beginning with the concept of defining target regions based on HP ^{3}He MRI, conducting bronchoscopic sampling of those regions, processing the resulting physical samples, digitizing the results, and quantifying cell counts on those images. We have thus used this pilot population to develop and test a reproducible workflow for further studies of this nature in asthma and other obstructive lung diseases, using HP ^{3}He MRI to provide a guide and context for targeted sampling, gaining valuable expertise and lessons learned in the process.

7.5 CONCLUSION

We have developed a workflow for using HP ^{3}He MRI to guide targeted sampling of ventilation defect and well-ventilated control sites in asthma, thereby enabling the direct assessment of airway morphology and cellular activity in the context of their functional significance. We showed that granulocyte levels were elevated in sites of ventilation defect, confirming and adding a regional element to previously published work, and conducted a preliminary analysis of paired samples in a pilot population of asthma subjects. Future work will expand this process to a wider population of asthma subjects and incorporate additional factors such as degree of regional VDP, analysis of protein counts in lavage and of brushings, and the use of corticosteroids, to provide a more refined analysis of these markers in the context of ventilation heterogeneity.

8 SUMMARY AND FUTURE WORK

8.1 SUMMARY

This dissertation is centered around the idea that ventilation patterns observed on HP ^{3}He MRI in asthma are meaningful as both as a clinically useful measure of disease severity and propensity for exacerbation and as a framework for a better understanding of the functional significance of mechanisms of airway obstruction.

We first established a basic connection between ventilation defects and clinical measures by showing associations between whole-lung VDP and a history of severe asthma-related outcomes using extant VDP results calculated as part of a previous study. Along the way, we assessed correlations between VDP and conventional measures of spirometry and inflammatory response, and found in a multivariate model incorporating these factors that VDP was still the most influential component associated with a history of exacerbation.

With this fundamental result established, we conducted a prospective study of whole-lung VDP as a predictor of exacerbation frequency in the two years following imaging, where we broadened the definition of exacerbation to encompass events that led to corticosteroid use but not necessarily to an ED visit or hospital stay. We implemented software designed in our lab to conduct a comprehensive VDP analysis on this longitudinal study population. Despite the inclusion of lower-severity exacerbations, VDP proved a significant predictor both of binary exacerbation incidence (analogous to the previous study) and exacerbation frequency, that is, cumulative exacerbations over

the two-year time period. In addition, we found that incorporating history of severe exacerbation – a less strong but still significant predictor – with VDP into a two-part decision tree model was remarkably effective at selecting subjects who would go on to experience a high frequency of exacerbation.

We then moved from whole-lung VDP to consider its use as a regional indicator of functional significance, assessing lobar and segmental VDP in the context of mucus plugs identified on CT, a phenomenon characteristic of asthma. We found that regional measures of VDP were associated with mucus plugging. With targeted asthma therapies on the verge of entering the mainstream, multiple varieties of which specifically target pathways associating with mucus hypersecretion, it is imperative to develop methods of assessing suitability for a potentially very costly therapy and evaluating treatment response.

Finally, we used image-guided bronchoscopy to establish the feasibility of targeted sampling of poorly ventilated regions vs. well-ventilated control sites and assessments of inflammatory markers on bronchoalveolar lavage, and difference in morphology and markers of injury, cell proliferation, and inflammatory response on histology. We set up a processing pipeline from imaging to bronchoscopy to analysis of microscopy and conducted preliminary analyses in a pilot population of asthmatics.

8.2 FUTURE WORK

8.2.1 Outcomes

The primary outcomes-based results in this work were centered around imaging obtained at the baseline timepoint of the Longitudinal population. However, this population contains

substantial imaging data that has yet to be fully analyzed, including MRI obtained after respiratory symptoms, CT and MRI at the three-year exit visit, and the post-bronchodilator MRI, none of which were utilized in this work. Finally, our existing image analysis pipeline enables a more nuanced analysis of ventilation distribution (i.e. quantitation of high-, medium-, and low-ventilation regions in addition to ventilation defects) that may shed additional light on the role of ventilation heterogeneity in asthma. Further analysis of this rich dataset may further bolster understanding of asthma disease progression and establish MRI as a biomarker of disease severity and propensity for exacerbation.

8.2.2 Regional Analysis

The techniques and workflow established here to assess the regional functional significance of mucus plugs may be extended to any biomarker that is assessed on a regional basis. Small airways trapping and bronchodilator reversibility, for example, could all be examined in the context of ventilation heterogeneity. Future work in this area could lead to a methodology capable of measuring multiple image-based biomarkers of airway obstruction together with their functional significance. This would be a fundamental technique for the development of imaging-based asthma phenotypes for use in selected patients for targeted therapies and for assessing response to those therapies both in the clinic and in as a secondary endpoint in clinical trials. Moreover, this regional imaging approach could easily be extended to other obstructive lung diseases such as COPD.

8.2.3 Image-Guided Bronchoscopy

We have established a foundational end-to-end workflow for the quantification of cellular activity in BAL and biopsy samples obtained via image-guided bronchoscopy. We will extend this pipeline to a larger population of asthmatics from the Longitudinal population,

building on our pilot population to a more comprehensive analysis of the biomarkers of cellular activity in regions of ventilation defect.

9 PUBLICATIONS AND PRESENTATIONS

9.1 ACCEPTED PEER-REVIEWED JOURNAL ARTICLES

- Jessica M. Oakes, **David Mummy,** Kamran Poorbahrami, Wei Zha, and Sean B. Fain. “Patient-Specific Computational Simulations of Hyperpolarized 3He MRI Ventilation Defects in Healthy and Asthmatic Subjects”. *IEEE Transactions in Biomedical Engineering* [in press].
- Zha, Wei, Stanley J. Kruger, Robert V. Cadman, **David G. Mummy,** Michael D. Evans, Scott K. Nagle, Loren C. Denlinger, Nizar N. Jarjour, Ronald L. Sorkness, and Sean B. Fain. “Regional Heterogeneity of Lobar Ventilation in Asthma Using Hyperpolarized Helium-3 MRI.” *Academic Radiology* 25, no. 2 (2018): 169-178.
- **David G. Mummy,** Stanley J. Kruger, Wei Zha, Ronald L. Sorkness, Nizar N. Jarjour, Mark L. Scheibler, Loren C. Denlinger, Michael D. Evans, Sean B. Fain. “Ventilation defect percent in helium-3 magnetic resonance imaging as a biomarker of severe outcomes in asthma.” Journal of Allergy and Clinical Immunology 141.3 (2018).
- E. Adamson, K. Ludwig, **D. Mummy,** S.B. Fain. “Magnetic resonance imaging with hyperpolarized agents: methods and applications”. *Physics in Medicine and Biology* (2017). doi: 10.1088/1361-6560/aa6be8.
- Wei Zha, David J. Niles, Stanley J. Kruger, Bernard J. Dardzinski, Robert V. Cadman, **David G. Mummy,** Scott K. Nagle, and Sean B. Fain. “Semiautomated Ventilation Defect Quantification in Exercise-induced Bronchoconstriction Using Hyperpolarized Helium-3 Magnetic Resonance Imaging: A Repeatability Study”. *Academic Radiology* (2016).
- V. Shankaran, **D. Mummy,** L. Koepl, A. Bansal, D. Mirick, E. Yu, R. Morlock, S. Ogale, and S. Ramsey. “Survival and lifetime costs associated with first-line bevacizumab use in older patients with metastatic colorectal cancer”. *Oncologist* 19:892-899, 2014
- V. Shankaran, **D. Mummy,** L. Koepl, D. Blough, Y. M. Yim, E. Yu, S. Ramsey. “Adverse events associated with Bevacizumab and chemotherapy in older patients with metastatic colorectal cancer”. *Clin Colorectal Cancer* 2013; 12(3): 204213
- B. Goulart, C. Reyes, C. Fedorenko, **D. Mummy**, S. Satram-Hoang, L. Koepl, D. Blough, S. Ramsey. “Referral and treatment patterns among patients with stages III and IV non-small cell lung cancer”. *Journal of Oncology Practice*, 9, 42-50. doi:10.1200/JOP.2012.000640
- B. Goulart, M. Bensink, **D. Mummy**, S. Ramsey. “Lung cancer screening with lowdose computed tomography: costs, national expenditures, and cost-

effectiveness". *Journal of the National Comprehensive Cancer Network: JNCCN*. 01/2012; 10(2): 267-275.

9.2 BOOK CHAPTERS

- "Asthma." **David G. Mummy**, Wei Zha, Ronald L. Sorkness, Sean B. Fain. *MRI of the Lung*, Hans-Ulrich Kauczor and Mark Oliver Wielputz, Eds. Springer, 2018.
- "Hyperpolarized Gas MRI of the Lung in Asthma." Sean B. Fain, **David G. Mummy**, Ronald L. Sorkness. *Hyperpolarized and Inert Gas MRI: From Technology to Application in Research and Medicine*, Mitchell S. Albert and Francis T. Hane, Eds. Academic Press, 2016.

9.3 MANUSCRIPTS IN PROGRESS

- **David G. Mummy**, Eleanor Dunican, Wei Zha, Michael Evans, Scott Nagle, Mark Schiebler, Ronald L. Sorkness, Nizar N. Jarjour, Loren C. Denlinger, Sean B. Fain. "Central airway mucus plugging on CT is associated with ventilation heterogeneity on hyperpolarized gas MRI in asthma."
- **David G. Mummy**, Katherine J. Carey, Michael D. Evans, Wei Zha, Ronald L. Sorkness, Mark L. Schiebler, Loren C. Denlinger, Nizar N. Jarjour, Sean B. Fain. "Ventilation defects on hyperpolarized helium3- MRI are predictive of 2-year exacerbation frequency in asthma"
- **David G. Mummy,** Shannon Kehoe, Scott Aesif, Ronald Sorkness, Nizar Jarjour, Mark Schiebler, Michael Evans, Loren Denlinger, Sean Fain. "Image-guided bronchoscopy of regional ventilation heterogeneity in asthma as a means of assessing localized inflammatory response: preliminary results."

Reference

1. Moore, W.C., et al., *Characterization of the severe asthma phenotype by the National Heart, Lung, and Blood Institute's Severe Asthma Research Program.* J Allergy Clin Immunol, 2007. **119**(2): p. 405-13.
2. Akinbami, L., et al., *Trends in Asthma Prevalence, Health Care Use, and Mortality in the United States, 2001-2010*. 2012, National Center for Health Statistics.
3. Weinberger, S.E., B.A. Cockrill, and J. Mandel, *Principles of pulmonary medicine*. 6th ed. 2014, Philadelphia, PA: Elsevier/Saunders. x, 404 p.
4. Sorkness, R.L., et al., *Lung function in adults with stable but severe asthma: air trapping and incomplete reversal of obstruction with bronchodilation.* Journal of applied physiology, 2008. **104**(2): p. 394-403.
5. Levitzky, M.G., *Pulmonary physiology*. 8th ed. 2013, New York: McGraw-Hill. p.
6. Bice, J.B., E. Leechawengwongs, and A. Montanaro, *Biologic targeted therapy in allergic asthma.* Annals of Allergy Asthma & Immunology, 2014. **112**(2): p. 108-115.
7. Moore, W.C., et al., *Characterization of the severe asthma phenotype by the national heart, lung, and blood institute's severe asthma research program.* Journal of Allergy and Clinical Immunology, 2007. **119**(2): p. 405-413.
8. Lotvall, J., et al., *Asthma endotypes: A new approach to classification of disease entities within the asthma syndrome.* Journal of Allergy and Clinical Immunology, 2011. **127**(2): p. 355-360.
9. Samee, S., et al., *Imaging the lungs in asthmatic patients by using hyperpolarized helium-3 magnetic resonance: assessment of response to methacholine and exercise challenge.* Journal of Allergy and Clinical Immunology, 2003. **111**(6): p. 1205-1211.
10. Mugler, J.P. and T.A. Altes, *Hyperpolarized 129Xe MRI of the human lung.* Journal of Magnetic Resonance Imaging, 2013. **37**(2): p. 313-331.
11. Berend, N., C.M. Salome, and G.G. King, *Mechanisms of airway hyperresponsiveness in asthma.* Respirology, 2008. **13**(5): p. 624-631.
12. Miglioretti, D.L., et al., *The use of computed tomography in pediatrics and the associated radiation exposure and estimated cancer risk.* JAMA pediatrics, 2013. **167**(8): p. 700-707.
13. Hurwitz, L.M., et al., *Radiation dose from contemporary cardiothoracic multidetector CT protocols with an anthropomorphic female phantom: implications for cancer induction.* Radiology, 2007. **245**(3): p. 742-750.
14. Dunican, E.M., et al., *Mucus plugs in patients with asthma linked to eosinophilia and airflow obstruction.* The Journal of clinical investigation, 2018. **128**(3).
15. Howarth, D.M., et al., *99mTc technegas ventilation and perfusion lung scintigraphy for the diagnosis of pulmonary embolus.* Journal of Nuclear Medicine, 1999. **40**(4): p. 579.
16. Newman, S.P., et al., *Radionuclide imaging technologies and their use in evaluating asthma drug deposition in the lungs.* Advanced drug delivery reviews, 2003. **55**(7): p. 851-867.
17. Melo, M.F.V., et al., *Quantification of regional ventilation-perfusion ratios with PET.* The Journal of Nuclear Medicine, 2003. **44**(12): p. 1982.
18. Chen, Q., et al., *Oxygen enhanced MR ventilation imaging of the lung.* Magnetic Resonance Materials in Physics, Biology and Medicine, 1998. **7**(3): p. 153-161.
19. Hatabu, H., et al., *Pulmonary ventilation: dynamic MRI with inhalation of molecular oxygen.* European journal of radiology, 2001. **37**(3): p. 172-178.

20. Rinck, P., S. Petersen, and P. Lauterbur. *NMR-imaging von fluorhaltigen substanzen*. in *RöFo-Fortschritte auf dem Gebiet der Röntgenstrahlen und der bildgebenden Verfahren*. 1984. © Georg Thieme Verlag Stuttgart· New York.
21. Ruiz‐Cabello, J., et al., *Fluorine (19F) MRS and MRI in biomedicine.* NMR in Biomedicine, 2011. **24**(2): p. 114-129.
22. Halaweish, A.F., et al., *Perfluoropropane gas as a magnetic resonance lung imaging contrast agent in humans.* Chest, 2013. **144**(4): p. 1300-1310.
23. van Beek, E.J., et al., *Functional MRI of the lung using hyperpolarized 3‐helium gas.* Journal of Magnetic Resonance Imaging, 2004. **20**(4): p. 540-554.
24. Altes, T.A., et al., *Hyperpolarized 3He MR lung ventilation imaging in asthmatics: Preliminary findings.* Journal of Magnetic Resonance Imaging, 2001. **13**(3): p. 378-384.
25. Svenningsen, S., et al., *What are ventilation defects in asthma?* Thorax, 2014. **69**(1): p. 63-71.
26. Fain, S.B., et al., *Evaluation of Structure-Function Relationships in Asthma using Multidetector CT and Hyperpolarized He-3 MRI.* Academic Radiology, 2008. **15**(6): p. 753-762.
27. Zha, W., et al., *Semiautomated Ventilation Defect Quantification in Exercise-induced Bronchoconstriction Using Hyperpolarized Helium-3 Magnetic Resonance Imaging: A Repeatability Study.* Academic Radiology, 2016.
28. Thomen, R.P., et al., *Regional ventilation changes in severe asthma after bronchial thermoplasty with 3He MR imaging and CT.* Radiology, 2014. **274**(1): p. 250-259.
29. Woodhouse, N., et al., *Combined helium‐3/proton magnetic resonance imaging measurement of ventilated lung volumes in smokers compared to never‐smokers.* Journal of magnetic resonance imaging, 2005. **21**(4): p. 365-369.
30. Kirby, M., et al., *Quantitative evaluation of hyperpolarized helium-3 magnetic resonance imaging of lung function variability in cystic fibrosis.* Academic radiology, 2011. **18**(8): p. 1006-1013.
31. Salerno, M., et al., *Emphysema: hyperpolarized helium 3 diffusion MR imaging of the lungs compared with spirometric indexes—initial experience.* Radiology, 2002. **222**(1): p. 252-260.
32. Sukstanskii, A. and D. Yablonskiy, *Lung morphometry with hyperpolarized 129Xe: theoretical background.* Magnetic resonance in medicine, 2012. **67**(3): p. 856-866.
33. Fain, S.B., et al., *Detection of age-dependent changes in healthy adult lungs with diffusion-weighted 3He MRI.* Academic radiology, 2005. **12**(11): p. 1385-1393.
34. Chang, Y.V., *MOXE: a model of gas exchange for hyperpolarized 129Xe magnetic resonance of the lung.* Magnetic resonance in medicine, 2013. **69**(3): p. 884-890.
35. Qing, K., et al., *Assessment of lung function in asthma and COPD using hyperpolarized 129Xe chemical shift saturation recovery spectroscopy and dissolved‐phase MRI.* NMR in biomedicine, 2014. **27**(12): p. 1490-1501.
36. Qing, K., et al., *Regional mapping of gas uptake by blood and tissue in the human lung using hyperpolarized xenon‐129 MRI.* Journal of Magnetic Resonance Imaging, 2014. **39**(2): p. 346-359.
37. Gentile, T.R., et al., *Demonstration of a compact compressor for application of metastability‐exchange optical pumping of 3He to human lung imaging.* Magnetic Resonance in Medicine: An Official Journal of the International Society for Magnetic Resonance in Medicine, 2000. **43**(2): p. 290-294.
38. Walker, T.G. and W. Happer, *Spin-exchange optical pumping of noble-gas nuclei.* Reviews of Modern Physics, 1997. **69**(2): p. 629.

39. Denlinger, L.C., et al., *Lower airway rhinovirus burden and the seasonal risk of asthma exacerbation.* American journal of respiratory and critical care medicine, 2011. **184**(9): p. 1007-1014.
40. Jarjour, N.N., et al., *Severe asthma: lessons learned from the national heart, lung, and blood institute severe asthma research program.* American journal of respiratory and critical care medicine, 2012. **185**(4): p. 356-362.
41. Society, A.T., *Proceedings of the ATS workshop on refractory asthma: current understanding, recommendations, and unanswered questions.* Am. J. Respir. Crit. Care Med., 2000. **162**: p. 2341-2351.
42. Wanger, J., et al., *Standardisation of the measurement of lung volumes.* European respiratory journal, 2005. **26**(3): p. 511-522.
43. Miller, M.R., et al., *Standardisation of spirometry.* European respiratory journal, 2005. **26**(2): p. 319-338.
44. Hankinson, J.L., J.R. Odencrantz, and K.B. Fedan, *Spirometric reference values from a sample of the general US population.* American journal of respiratory and critical care medicine, 1999. **159**(1): p. 179-187.
45. Stocks, J. and P.H. Quanjer, *Reference values for residual volume, functional residual capacity and total lung capacity. ATS Workshop on Lung Volume Measurements. Official Statement of The European Respiratory Society.* European Respiratory Journal, 1995. **8**(3): p. 492-506.
46. Quanjer, P.H., et al., *Multi-ethnic reference values for spirometry for the 3–95-yr age range: the global lung function 2012 equations*. 2012, Eur Respiratory Soc.
47. Mets, O.M., et al., *Variation in quantitative CT air trapping in heavy smokers on repeat CT examinations.* European radiology, 2012. **22**(12): p. 2710-2717.
48. Busacker, A., et al., *A multivariate analysis of risk factors for the air-trapping asthmatic phenotype as measured by quantitative CT analysis.* Chest, 2009. **135**(1): p. 48-56.
49. Kirby, M., et al., *COPD: do imaging measurements of emphysema and airway disease explain symptoms and exercise capacity?* Radiology, 2015. **277**(3): p. 872-880.
50. Kirby, M., et al., *Hyperpolarized 3He ventilation defects used to predict pulmonary exacerbations in mild to moderate chronic obstructive pulmonary disease.* Radiology, 2014. **273**(3): p. 887-896.
51. Ebner, L., et al., *The role of hyperpolarized 129xenon in MR imaging of pulmonary function.* Eur J Radiol, 2017. **86**: p. 343-352.
52. Friedman, J.H., *Greedy function approximation: a gradient boosting machine.* Annals of statistics, 2001: p. 1189-1232.
53. Ridgeway, G., *The gbm package. Generalized boosted regression models (Documentation on the R Package 'gbm', version 1.6–3.)*. 2015.
54. de Lange, E.E., et al., *Evaluation of asthma with hyperpolarized helium-3 MRI.* Chest, 2006. **130**(4): p. 1055-1062.
55. Altes, T.A., et al., *Clinical correlates of lung ventilation defects in asthmatic children.* Journal of Allergy and Clinical Immunology, 2016. **137**(3): p. 789-796. e7.
56. Kruger, S.J., et al., *Hyperpolarized Helium‐3 MRI of exercise‐induced bronchoconstriction during challenge and therapy.* Journal of Magnetic Resonance Imaging, 2014. **39**(5): p. 1230-1237.
57. Mummy, D.G., et al., *Ventilation defect percent in helium-3 magnetic resonance imaging as a biomarker of severe outcomes in asthma.* Journal of Allergy and Clinical Immunology, 2018. **141**(3): p. 1140-1141. e4.
58. Zha, W., et al., *Regional Heterogeneity of Lobar Ventilation in Asthma Using Hyperpolarized Helium-3 MRI.* Academic radiology, 2017.
59. Teague, W.G., N.J. Tustison, and T.A. Altes, *Ventilation heterogeneity in asthma.* Journal of Asthma, 2014. **51**(7): p. 677-684.

60. Downie, S.R., et al., *Ventilation heterogeneity is a major determinant of airway hyperresponsiveness in asthma, independent of airway inflammation.* Thorax, 2007.
61. Svenningsen, S., et al., *What are ventilation defects in asthma?* Thorax, 2013: p. thoraxjnl-2013-203711.
62. Carroll, N., S. Mutavdzic, and A. James, *Increased mast cells and neutrophils in submucosal mucous glands and mucus plugging in patients with asthma.* Thorax, 2002. **57**(8): p. 677-682.
63. Rogers, D.F., *Airway mucus hypersecretion in asthma: an undervalued pathology?* Current opinion in pharmacology, 2004. **4**(3): p. 241-250.
64. Aikawa, T., et al., *Marked goblet cell hyperplasia with mucus accumulation in the airways of patients who died of severe acute asthma attack.* Chest, 1992. **101**(4): p. 916-21.
65. Ortega, H.G., et al., *Mepolizumab treatment in patients with severe eosinophilic asthma.* New England Journal of Medicine, 2014. **371**(13): p. 1198-1207.
66. Castro, M., et al., *Reslizumab for inadequately controlled asthma with elevated blood eosinophil counts: results from two multicentre, parallel, double-blind, randomised, placebo-controlled, phase 3 trials.* The Lancet Respiratory Medicine, 2015. **3**(5): p. 355-366.
67. Castro, M., et al., *Benralizumab, an anti-interleukin 5 receptor α monoclonal antibody, versus placebo for uncontrolled eosinophilic asthma: a phase 2b randomised dose-ranging study.* The Lancet Respiratory Medicine, 2014. **2**(11): p. 879-890.
68. Zeki, A.A., et al., *Simvastatin inhibits goblet cell hyperplasia and lung arginase in a mouse model of allergic asthma: a novel treatment for airway remodeling?* Translational Research, 2010. **156**(6): p. 335-349.
69. de Freitas Alves, C., et al., *The effects of proresolution of ellagic acid in an experimental model of allergic airway inflammation.* Mediators of inflammation, 2013. **2013**.
70. Galbán, C.J., et al., *Computed tomography-based biomarker provides unique signature for diagnosis of COPD phenotypes and disease progression.* Nature medicine, 2012. **18**(11): p. 1711-1715.
71. Svenningsen, S., et al., *Hyperpolarized 3He and 129Xe MRI: Differences in asthma before bronchodilation.* Journal of Magnetic Resonance Imaging, 2013. **38**(6): p. 1521-1530.
72. Costella, S., et al., *Regional pulmonary response to a methacholine challenge using hyperpolarized 3He magnetic resonance imaging.* Respirology, 2012. **17**(8): p. 1237-1246.
73. Tzeng, Y.-S., K. Lutchen, and M. Albert, *The difference in ventilation heterogeneity between asthmatic and healthy subjects quantified using hyperpolarized 3He MRI.* Journal of applied physiology, 2009. **106**(3): p. 813-822.
74. Greenblatt, E.E., et al., *Pendelluft in the bronchial tree.* Journal of Applied Physiology, 2014. **117**(9): p. 979-988.
75. Young, H.M., et al., *Oscillometry and Pulmonary MRI Measurements of Ventilation Heterogeneity in Obstructive Lung Disease: Relationship to Quality of Life and Disease Control.* Journal of Applied Physiology, 2018.
76. Haldar, P., et al., *Cluster analysis and clinical asthma phenotypes.* American journal of respiratory and critical care medicine, 2008. **178**(3): p. 218-224.
77. de Groot, J.C., et al., *Clinical profile of patients with adult-onset eosinophilic asthma.* ERJ open research, 2016. **2**(2): p. 00100-2015.
78. Guilbert, T.W., L.B. Bacharier, and A.M. Fitzpatrick, *Severe asthma in children.* The Journal of Allergy and Clinical Immunology: In Practice, 2014. **2**(5): p. 489-500.

79. Svenningsen, S., et al., *Sputum eosinophilia and magnetic resonance imaging ventilation heterogeneity in severe asthma.* American journal of respiratory and critical care medicine, 2018. **197**(7): p. 876-884.
80. Moore, W.C., et al., *Safety of investigative bronchoscopy in the Severe Asthma Research Program.* Journal of Allergy and Clinical Immunology, 2011. **128**(2): p. 328-336. e3.